NASA/TP-2004-212024

Heat Shielding Characteristics and Thermostructural Performance of a Superalloy Honeycomb Sandwich Thermal Protection System (TPS)

William L. Ko
NASA Dryden Flight Research Center
Edwards, California

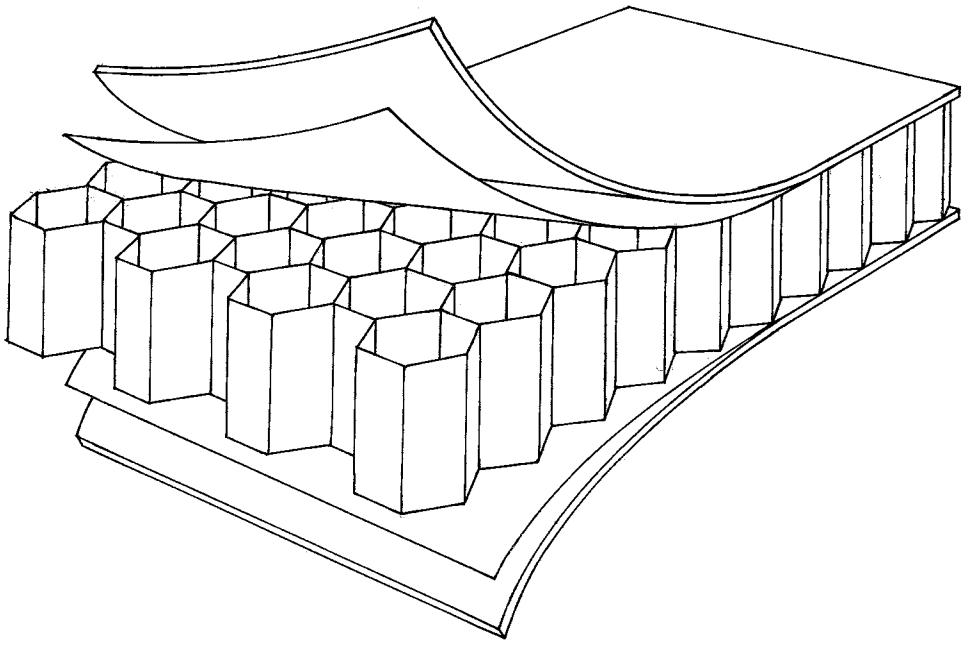

May 2004

The NASA STI Program Office…in Profile

Since its founding, NASA has been dedicated to the advancement of aeronautics and space science. The NASA Scientific and Technical Information (STI) Program Office plays a key part in helping NASA maintain this important role.

The NASA STI Program Office is operated by Langley Research Center, the lead center for NASA's scientific and technical information. The NASA STI Program Office provides access to the NASA STI Database, the largest collection of aeronautical and space science STI in the world. The Program Office is also NASA's institutional mechanism for disseminating the results of its research and development activities. These results are published by NASA in the NASA STI Report Series, which includes the following report types:

- TECHNICAL PUBLICATION. Reports of completed research or a major significant phase of research that present the results of NASA programs and include extensive data or theoretical analysis. Includes compilations of significant scientific and technical data and information deemed to be of continuing reference value. NASA's counterpart of peer-reviewed formal professional papers but has less stringent limitations on manuscript length and extent of graphic presentations.

- TECHNICAL MEMORANDUM. Scientific and technical findings that are preliminary or of specialized interest, e.g., quick release reports, working papers, and bibliographies that contain minimal annotation. Does not contain extensive analysis.

- CONTRACTOR REPORT. Scientific and technical findings by NASA-sponsored contractors and grantees.

- CONFERENCE PUBLICATION. Collected papers from scientific and technical conferences, symposia, seminars, or other meetings sponsored or cosponsored by NASA.

- SPECIAL PUBLICATION. Scientific, technical, or historical information from NASA programs, projects, and missions, often concerned with subjects having substantial public interest.

- TECHNICAL TRANSLATION. English-language translations of foreign scientific and technical material pertinent to NASA's mission.

Specialized services that complement the STI Program Office's diverse offerings include creating custom thesauri, building customized databases, organizing and publishing research results…even providing videos.

For more information about the NASA STI Program Office, see the following:

- Access the NASA STI Program Home Page at ***http://www.sti.nasa.gov***

- E-mail your question via the Internet to help@sti.nasa.gov

- Fax your question to the NASA Access Help Desk at (301) 621-0134

- Telephone the NASA Access Help Desk at (301) 621-0390

- Write to:
  NASA Access Help Desk
  NASA Center for AeroSpace Information
  7121 Standard Drive
  Hanover, MD 21076-1320

NASA/TP-2004-212024

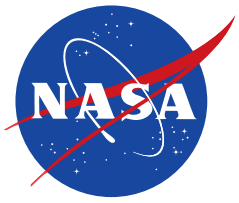

Heat Shielding Characteristics and Thermostructural Performance of a Superalloy Honeycomb Sandwich Thermal Protection System (TPS)

William L. Ko
NASA Dryden Flight Research Center
Edwards, California

National Aeronautics and
Space Administration

Dryden Flight Research Center
Edwards, California 93523-0273

May 2004

NOTICE

Use of trade names or names of manufacturers in this document does not constitute an official endorsement of such products or manufacturers, either expressed or implied, by the National Aeronautics and Space Administration.

Available from the following:

NASA Center for AeroSpace Information (CASI)
7121 Standard Drive
Hanover, MD 21076-1320
(301) 621-0390

National Technical Information Service (NTIS)
5285 Port Royal Road
Springfield, VA 22161-2171
(703) 487-4650

CONTENTS

ABSTRACT

Heat-transfer, thermal bending, and mechanical buckling analyses have been performed on a superalloy "honeycomb" thermal protection system (TPS) for future hypersonic flight vehicles. The studies focus on the effect of honeycomb cell geometry on the TPS heat-shielding performance, honeycomb cell wall buckling characteristics, and the effect of boundary conditions on the TPS thermal bending behavior.

The results of the study show that the heat-shielding performance of a TPS panel is very sensitive to change in honeycomb core depth, but insensitive to change in honeycomb cell cross-sectional shape. The thermal deformations and thermal stresses in the TPS panel are found to be very sensitive to the edge support conditions. Slight corrugation of the honeycomb cell walls can greatly increase their buckling strength.

NOMENCLATURE

a	depth of honeycomb core, or length of a rectangular plate, in.
a'	= 1a, 1.5a, 2a, modified depth of honeycomb core, in.
$A_c^{(i)}$	cross-sectional area (perpendicular to the cell axis) of honeycomb cell type i, in^2
$A_w^{(i)}$	cross-sectional area (perpendicular to the cell axis) of cell walls of honeycomb cell type i, in^2
b	width of a rectangular plate, in.
b_i	length of free side of type i honeycomb cell cross section, in.
b'	length of bonded double side of TPS cell cross section, in.
$\tilde{b}$	= 5c, corrugation length of corrugated side of corrugated cell cross section, in.
c	length of one corrugation leg, in.
d_i	size of type i honeycomb cell (maximum diagonal of the cell cross section), in.
D_i	bending stiffness of wall panel of type i honeycomb cell, in-lb
E	Young's modulus, lb/in^2
$F_{\boldsymbol{ij}}$	radiation view factor, defined as the fraction of radiant heat leaving radiation element ***i*** and incident on radiation element ***j***
G	shear modulus, lb/in^2
h_c	corrugation depth (twice the amplitude of corrugation wave), in.
i	index (1, 2, 3,...) associated with type i honeycomb cell geometry: i = 1 for right hexagonal cell; i = 2 for square cell; i = 3 for TPS flat cell walls; i = 4 for TPS corrugated cell walls

i index (1, 2, 3,...) associated with radiation element ***i***

j index (1, 2, 3,...) associated with radiation element ***j***

JLOC joint location

k $= \frac{b_i^2}{\pi^2 D_i}(N_z)_{cr}^{(i)}$, buckling coefficient for a rectangular plate with aspect ratio a/b_i under uniaxial compression in *a* direction

l side length of square honeycomb-core sandwich TPS panel, in.

m number of buckled half-waves in rectangular plate longitudinal direction

n number of buckled half-waves in rectangular plate lateral direction

$(N_z)_{cr}^{(i)}$ classical compressive buckling load intensity in the *z* direction of the weakest rectangular wall panel of type *i* honeycomb cell, lb/in

p one-half of corrugation pitch, $\sqrt{c^2 - h_c^2}$, in.

q aerodynamic pressure over outer surface of honeycomb-core sandwich TPS panel, lb/in^2

$q_{cr}^{(i)}$ critical value of q at buckling for type *i* honeycomb cell walls, lb/in^2

SPAR Structural Performance and Resizing (finite-element computer program)

STS space transportation system

t time, sec

t_c honeycomb cell wall thickness, in.

$\tilde{t}_c$ corrugated honeycomb cell wall thickness, in.

t_s sandwich face sheet thickness, in.

T_l inner face sheet temperature, °F

TPS thermal protection system

$T(t)$ transient surface temperature over outer surface of honeycomb-core sandwich TPS panel, °F

T_u outer face sheet temperature, °F

v Poisson’s ratio

w_e deflection at sandwich panel edge midpoint, in.

w_{max} maximum deflection at sandwich panel center, in.

W weight, lb

x, y, z rectangular Cartesian coordinates

α coefficient of thermal expansion, in/in–°F

ΔT $= T_u - T_l$, difference between outer and inner face sheet temperatures, °F

θ corrugation angle, deg

ρ_c density of material used for honeycomb core and sandwich face sheets, lb/in^3

ρ_i effective density of honeycomb core with type *i* cell geometry, lb/in^3

$\rho_{sw}^{(i)}$ effective density of sandwich panel with type *i* honeycomb cell geometry, lb/in^3

σ_x stress in x direction induced in the face sheets, lb/in^2

σ_y stress in y direction induced in the face sheets, lb/in^2

σ_z compressive stress in *z* direction in the honeycomb cell walls induced by the surface pressure *q*

$(\sigma_z)_{cr}^{(i)}$ compressive stress in *z* direction in the honeycomb cell walls at the buckling of the weakest cell wall

Subscripts:

$( )_{cr}$ critical value at buckling

$( )_i$ associated with type *i* honeycomb cell geometry

Superscripts:

$( )^{(i)}$ associated with type *i* honeycomb cell geometry

INTRODUCTION

Hypersonic flight vehicles such as the Space Shuttle orbiter are subjected to severe aerodynamic heating during flight missions. A thermal protection system (TPS) made of low–thermal conductivity materials is used to insulate primary structures from overheating so that the vehicle can operate within the design temperature limit (ref. 1). Typical types of TPS include porous silica rigid “tiles” (ref. 2), flexible felt “blanket” (ref. 3), multiwalled titanium panels with dimpled cores (refs. 4, 5), and so forth. The main disadvantage of the rigid TPS tiles is the fragility of the materials used. After each mission, numerous tiles must be replaced because of surface damage incurred. To eliminate such repairs, a superalloy “honeycomb” TPS is currently being considered for future space transportation systems (STSs) (refs. 6, 7). The honeycomb construction provides low density and low thermal conductivity through the TPS thickness. The superalloy TPS is capable of functioning at high temperatures (ref. 8).

A TPS is exposed to high temperatures on the outer surface and to relatively lower temperatures on the inner surface facing the cooler substructures. This thermal gradient across the TPS thickness will induce thermal bending moment, causing the TPS panel to bulge outwardly. A highly efficient TPS could provide large temperature gradient across its depth; however, excess temperature gradient across the depth could induce excess thermal bending of the TPS panel, thus disturbing the local air flow. Therefore, proper trade studies must be exercised to design optimum honeycomb TPS structures. Also, the honeycomb TPS will be subjected to aerodynamic pressure loading, and cell walls must be stiff enough to withstand the air load without buckling.

This report presents the results of the heat-shielding and thermostructural analyses of honeycomb "sandwich" TPS panels that have different honeycomb cell geometries.

DESCRIPTION OF PROBLEM

Figure 1 shows a honeycomb-core sandwich TPS panel subjected to transient surface temperature, $T(t)$, and aerodynamic pressure, q, over its entire outer surface. The TPS panel is square with a side length of l, and is fabricated with two identical face sheets with a thickness of t_s and a honeycomb core with a depth of a. For a given material, the overall heat-shielding and thermostructural performances of the honeycomb TPS panel depend on the thickness of the face sheets, depth of the honeycomb core, thickness of the honeycomb cell walls, and size and shape of the honeycomb cells.

The first problem is to perform geometrical (shape) analysis of different candidate honeycomb cells that have the same effective density but different geometrical shapes. The second problem is to perform heat-transfer analysis of TPSs with different honeycomb cell geometry. The third problem is to perform the thermal bending analysis of the TPS panels subjected to one-sided heating and under different support conditions. The fourth problem is to perform comparative buckling analysis of different types of honeycomb cell wall panels under compressive surface air pressure.

HONEYCOMB STRUCTURES

This section presents the geometrical analysis of honeycomb cells with different geometry. The honeycomb TPS fabrication process also is described.

Honeycomb Construction

The honeycomb-core structure is fabricated using multiple layers of thin strips of metallic (or nonmetallic) foils joined together and properly deformed (ref. 9). The thin strips are bonded together first at equally spaced parallel zones (fig. 2). The equally spaced bonding zones on one side of each thin strip are staggered with respect to those on the opposite side. The bonded multiple sheet assembly then is pulled apart in the thickness direction through bending of the bonded and free junctures to form a final honeycomb structure (fig. 2). By modifying the width of the interfacial bonding belt zones and their spacing, and by pulling apart the multiple layers through bending deformations to a desired level, a family of different honeycomb cell geometry could be generated. Figure 3 shows the exploded view of the construction of a sandwich panel with upper and lower face sheets to be bonded to the honeycomb core through the brazing process.

Honeycomb Cells

Figure 4 shows four types of honeycomb cell geometry to be analyzed. The honeycomb cell wall thickness for the first three types is t_c. The first type is a right hexagonal cell (fig. 4(a)) with identical side lengths of b_1. The second type is a square cell (fig. 4(b)) with side lengths of b_2, which is modified from the right hexagonal cell by reducing the bonding interface length to a minimum of $\sqrt{2}t_c$. The third type is a distorted honeycomb cell with flat cell walls (fig. 4(c)). In this type of honeycomb cell, the bonded side length b' is slightly less than the free side length b_3, and the angle between the two adjacent free cell walls is adjusted to be 90 degrees.

The fourth geometry type is also a distorted honeycomb cell, but the free cell walls are corrugated (fig. 4(d)). Each corrugated wall has five corrugation legs. Cell wall thickness for the fourth type is either t_c or $\tilde{t}_c (\le t_c)$, which decreases with increasing corrugation depth, h_c, for maintaining constant core density (fig. 5). The third and fourth types of distorted honeycomb cells have the same linear dimensions (that is, identical b' and $b_4 = b_3$), and are the approximate cell geometry of the proposed superalloy TPS for a new STS. The size, $d_i (i = 1, 2, 3, 4)$, of each type of honeycomb cell is defined as the maximum diagonal of the cell cross section (fig. 4).

Effective Densities

If $A_c^{(i)}$ and $A_w^{(i)}$, respectively, are the cross-sectional areas (perpendicular to the cell axis) of honeycomb cell type *i* and its cell walls, then the effective density of honeycomb core with type *i* cell geometry, ρ_i (face sheets excluded), is given by the following:

$$\frac{\rho_i}{\rho_c} = \frac{A_w^{(i)}}{A_c^{(i)}} \quad ; \quad (i = 1, 2, 3, 4) \tag{1}$$

where ρ_c is the density of the material used for the honeycomb core and sandwich face sheets.

The density of the sandwich panel (including honeycomb core and face sheets) can be written as the following:

$$\frac{\rho_{sw}^{(i)}}{\rho_c} = \frac{A_w^{(t)} a + 2t_s A_c^{(i)}}{A_c^{(i)} a + 2t_s A_c^{(i)}} = \frac{\dfrac{\rho_i}{\rho_c} + \dfrac{2t_s}{a}}{1 + \dfrac{2t_s}{a}} \tag{2}$$

in which equation (1) was used. The weight *W* of the TPS panel is given by

$$W = \rho_{sw}^{(i)} l^2 (a + 2t_s) = l^2 \rho_c \left(2t_s + a \frac{\rho_i}{\rho_c} \right) \tag{3}$$

In the calculations of $A_w^{(i)}$, only one-half thickness of the cell wall was used because each of the cell wall panels is mutually shared by two adjacent cells. Namely, the unit cell wall thickness is $2t_c/2 = t_c$ for the bonded double walls and $t_c/2$ for the free walls. The effective densities for the four types of honeycomb cores can be written as follows (see the appendix for detailed calculations):

Right hexagonal cell (i = 1):

$$\frac{\rho_1}{\rho_c} = \frac{A_w^{(1)}}{A_c^{(1)}} = \frac{8\sqrt{3}t_c}{9b_1} = \frac{16\sqrt{3}t_c}{9d_1} \quad ; \quad b_1 = \frac{d_1}{2} \tag{4}$$

Square cell (i = 2):

$$\frac{\rho_2}{\rho_c} = \frac{A_w^{(2)}}{A_c^{(2)}} = 2\frac{t_c}{b_2} = 2\sqrt{2}\frac{t_c}{d_2} \quad ; \quad b_2 = \frac{\sqrt{2}}{2}d_2 \tag{5}$$

TPS cell (flat wall) (i = 3):

$$\frac{\rho_3}{\rho_c} = \frac{A_w^{(3)}}{A_c^{(3)}} = \frac{2}{5}(3+\sqrt{2})\frac{t_c}{b_3} = \frac{8\sqrt{2}}{15}(3+\sqrt{2})\frac{t_c}{d_3} \quad ; \quad b_3 = \frac{3\sqrt{2}}{8}d_3 \tag{6}$$

TPS cell (corrugated wall) (i = 4):

$$\frac{\rho_4}{\rho_c} = \frac{2}{5}\left(3\frac{\tilde{b}}{b_4}+\sqrt{2}\right)\frac{\tilde{t}_c}{b_4} = \frac{8\sqrt{2}}{15}\left(3\sqrt{1+\frac{256}{3}\frac{h_c^2}{d_4^2}}+\sqrt{2}\right)\frac{\tilde{t}_c}{d_4} \quad ; \quad b_4 = \frac{3\sqrt{2}}{8}d_4 \tag{7}$$

in which the following expression for corrugation length $\tilde{b}$ was used (fig. 5 and appendix):

$$\frac{\tilde{b}}{b_4} = \sqrt{1+24\frac{h_c^2}{b_4^2}} = \sqrt{1+\frac{256}{3}\frac{h_c^2}{d_4^2}} \tag{8}$$

Cell Sizes

To compare the heat-shielding and buckling performances, the size of honeycomb cells types 1, 2, and 4 are adjusted to have the same effective density as that of honeycomb cell type 3 (that is, $\rho_1 = \rho_2 = \rho_3 = \rho_4$). By equating equations (4) and (6), and equations (5) and (6), the cell sizes d_1 and d_2 are determined as

$$d_1 = \frac{10\sqrt{3}}{3\sqrt{2}(\sqrt{2}+3)}d_3 \tag{9}$$

$$d_2 = \frac{15}{4(\sqrt{2}+3)} d_3 \tag{10}$$

Figure 6 shows the plots of d_1 and d_2 as functions of d_3 based on equations (9) and (10). For the corrugated cell, by definition

$$d_4 = d_3 \tag{11}$$

and to maintain the same effective density (that is, $\rho_4 = \rho_3$), the corrugated cell wall thickness $\tilde{t}_c$ is reduced as the corrugation depth h_c increases according to the following equation (see appendix).

$$\frac{\tilde{t}_c}{t_c} = \frac{3+\sqrt{2}}{3\sqrt{1+24\dfrac{h_c^2}{b_4^2}}+\sqrt{2}} = \frac{3+\sqrt{2}}{3\sqrt{1+\dfrac{256}{3}\dfrac{h_c^2}{d_4^2}}+\sqrt{2}} \quad ; \quad b_4 = \frac{3\sqrt{2}}{8} d_4 \tag{12}$$

Figure 7 shows the corrugation angle, θ, plotted as a function of corrugation depth h_c/t_c; figure 8 shows the corrugated cell wall thickness $\tilde{t}_c/t_c$ decreases with the increasing corrugation depth h_c/t_c.

Numerical Input Values

A typical candidate TPS panel for a new STS has the following dimensions:

a = 0.488 in.

d_3 = 0.25 in.

l = 16.7 in.

t_s = 0.06 in.

t_c = 0.0015 in.

which gives a honeycomb core density of $\rho_3/\rho_c = 0.019976$ (face sheets excluded; eq. (1)) and a sandwich panel density of $\rho_{sw}^{(3)}/\rho_c = 0.043497$ (core plus face sheets; eq. (2)). For identical effective densities (that is, $\rho_1 = \rho_2 = \rho_3 = \rho_4 = 0.019976\rho_c$ or $\rho_{sw}^{(1)} = \rho_{sw}^{(2)} = \rho_{sw}^{(3)} = \rho_{sw}^{(4)} = 0.043497\rho_c$), the dimensions of the four types of honeycomb cells considered are listed in table 1, where for the corrugated cell, the range of corrugation depths $h_c/t_c = 0\text{–}6$ covers h_c/t_c = 0, 0.50, 1.00, 1.50, 1.75, 2.00, 2.25, 3.00, 3.50, 4.00, 4.50, 5.00, 5.50, 6.00.

Table 1. Dimensions of different honeycomb cells with identical effective core densities ($\rho_1 = \rho_2 = \rho_3 = \rho_4 = 0.019976\rho_c$).

Cell type (i)	b_i, in.	b', in.	d_i, in.	t_c, in.	$\tilde{t}_c$, in.	h_c/t_c	p, in.
Right hexagonal (i = 1)	0.1156	0.1156	0.2312	0.0015			
Square (i = 2)	0.1502	0	0.2124	0.0015			
TPS (flat) (i = 3)	0.1326	0.0625	0.2500	0.0015			
TPS (corrugated) (i = 4)	0.1326	0.0625	0.2500		eq (12)	0–6	0.0265

FINITE-ELEMENT ANALYSIS

This section describes the heat-transfer analysis of unit honeycomb cells of different geometry, thermal bending analysis of a honeycomb TPS panel, and core-depth-wise buckling analysis of honeycomb cell walls of different geometry. The TPS panel is assumed to be fabricated with superalloy Inconel 617 (Inco Alloys International, Inc., Huntington, West Virginia). The Structural Performance and Resizing (SPAR) finite-element computer program (ref. 10) was used in the three kinds of analyses.

Heat-Transfer Analysis

The heat-shielding performance of the honeycomb TPS panel can be studied by simply considering the heat transfer in a single honeycomb cell. Figure 9 shows the finite-element thermal models generated for the four types of honeycomb cells for the heat-transfer analysis. The upper and lower face sheets were modeled with K31 (ref. 10) triangular conduction elements with thickness t_s, and the honeycomb cell walls were modeled with quadrilateral K41 (ref. 10) conduction elements. Because each cell wall panel is shared by two adjacent cells, $t_c/2$ was used for the heat-transfer analysis as the thickness of K41 elements lying in the free-cell wall regions, and t_c for the thickness of K41 elements lying in the interbonded double-cell wall regions.

For internal radiation exchanges, three-nodes R31 (ref. 10) radiation elements and four-nodes R41 (ref. 10) radiation elements were attached respectively to the inner faces of K31 and K41 elements. The internal radiation view factors were computed using a VIEW program (ref. 10) incorporated into the SPAR program. Because the honeycomb cell is an enclosed structure, the “ENCLOSURE” command was used to correct the calculated radiation view factors so that the sum of the view factors from each element is equal to unity. Namely, if F_{ij} (i, j = 1, 2, 3,...) is the radiation view factor defined as the fraction of radiant heat leaving radiation element i and incident on radiation element j, then the “ENCLOSURE” command will impose the following condition for the final values of F_{ij}:

$$\sum_{j} F_{ij} = 1 \tag{13}$$

where the summation is taken over j for each given i.

Further, the command “UNOBSTRUCT”; “ALL” was used to define that all the internal radiation surfaces (or radiation elements) are nonobstructive. Reference 11 provided the thermal property data of the superalloy Inconel 617 for input to the thermal models. Table 2 shows the sizes of thermal models for the four types of honeycomb cells.

Table 2. Sizes of finite-element thermal models generated for different honeycomb cells.

Cell type (i)	JLOC	K31	K41	R31	R41
Right hexagonal ($i = 1$)	525	48	480	48	480
Square ($i = 2$)	441	40	400	40	400
TPS (flat) ($i = 3$)	525	48	480	48	480
TPS (corrugated) ($i = 4$)	525	48	480	48	480

For the heat input to the upper face sheet of the honeycomb cell, a heating rate of 16 °F/sec was used. This heating rate is comparable to the steepest stage of surface heating rate at a certain body point of a new type of STS during its mission. Because the surface heating is a temperature input instead of a heat-flux input, external radiation exchanges with space could be neglected. Furthermore, because of the tiny volume inside each honeycomb cell, both convection and conduction heat transfer of the interior air mass were neglected. This section studies the effect of honeycomb cell geometry on the heat-shielding performance of the TPS panel.

Thermal Bending Analysis

Figure 10 shows a quarter-panel finite-element model generated for the honeycomb TPS panel for thermal bending analysis. Because of symmetry with respect to the in-plane x- and y-axes, only one-quarter of the TPS panel was modeled. The commands “SYMMETRY PLANE = 1” and “SYMMETRY PLANE = 2” (ref. 10) were used to create the mirror images of the quarter-panel region, thereby simulating the whole panel.

Each face sheet is modeled with one layer of quadrilaterally combined membrane and bending E43 (ref. 10) elements, and the honeycomb core with a single layer of hexahedron (or brick) S81 (ref. 10) elements connecting the upper and lower face sheet E43 elements.

In the thermal bending analysis, the extensional and bending stiffness of the sandwich panel is assumed to be carried by the two face sheets, and the transverse shear stiffness by the honeycomb core. The TPS panel will be supported under the following different boundary conditions for comparing different degrees of thermal deformations and thermal stress fields induced in the TPS panel:

1. Fixed simply supported corners: four corners of the middle plane are simply supported and fixed.
2. Free simply supported corners: four corners of the middle plane are simply supported, but are allowed to move freely in the *x* and *y* directions.
3. Fixed clamped corners: clamped four corners are fixed.
4. Free clamped corners: clamped four corners are allowed to move freely in the *x* and *y* directions.
5. Fixed simply supported edges: four edges of the middle plane are simply supported and are fixed.
6. Free simply supported edges: four edges of the middle plane are simply supported and are allowed to move freely in the *x* and *y* directions.
7. Fixed clamped edges: clamped four edges are fixed.
8. Free clamped edges: clamped four edges are allowed to move freely in the *x* and *y* directions.

This method of simply supporting a sandwich panel is slightly different from simply supporting a solid flat plate (ref. 12). To simulate the fixed or free simply supported condition for the sandwich panel, pin-ended rigid rods were attached vertically to the panel edges (or corners) to connect the two face sheets (figs. 11(a)–(b)). Because the honeycomb core does not carry extensional or bending stiffness, edge support points cannot be attached to the honeycomb core. The midpoint of each rigid rod was pin-joined to a point (fixed or movable in the *x*-*y* plane) lying in the hypothetical panel middle plane (ref. 12). Each pin-ended rigid rod was modeled with two identical E22 (ref. 10) elements (beam elements for which the intrinsic stiffness matrixes are given). To simulate the rigidity of the rods, the extensional and the transverse shear stiffness of the E22 elements were made very large. The pin-joint condition at the face sheet edges was simulated by assigning zero values to the rotational spring constants in the stiffness matrix for the E22 elements. To simulate the pin-joint condition at the hypothetical middle plane, the three rotational constraints were eliminated. One node of each E22 element was connected to the associated node of E43 element, and the other node was connected to the hypothetical middle-plane point. For the fixed or free simply supported corners, only one pair of E22 elements was attached to one corner of the quarter-panel model.

For the fixed or free clamped edges (figs. 11(c)–(d)), the panel edges (or corners) were constrained to have zero transverse rotations. The sizes of the quarter-panel models for the honeycomb TPS are given below.

Table 3. Sizes of quarter-panel finite-element models for honeycomb TPS panel.

Support condition	JLOC	E22	E43	S81
Simply supported, clamped edges	1299	98	1152	576
Simply supported, clamped corners	1251	2	1152	576

The upper face sheet will be heated uniformly to temperature, T_u, of 800 °F and the lower sheet to temperature, T_l, of 450 °F. These temperature levels are similar to the temperatures across the TPS depth giving the maximum temperature gradient at a certain body point during a new STS mission. The material properties of the Inconel 617 were obtained from reference 11, and the effective elastic constants of Inconel 617 honeycomb core (with TPS cell geometry) were calculated using the formulae developed in reference 13. This section examines the panel deflections and the levels of the induced thermal stresses in the TPS panel under different support conditions.

Cell Wall Buckling Analysis

Compressive buckling behavior of a honeycomb panel subjected to surface aerodynamic pressure *q* (fig. 1) can be studied by simply considering the weakest cell wall panel of each type of honeycomb cell. Figure 12 shows the locations of the weakest cell wall panels analyzed, and figure 13 shows the corresponding finite-element models. For simplicity, the cell wall panel boundaries are simply supported. For the corrugated cell wall panel, two cases are considered: varying thickness $\tilde{t}_c$ to maintain constant density ($\rho_4 = \rho_3$); and constant panel thickness t_c (to determine how ρ_3 increases with increasing h_c).

Let σ_z be the compressive stress in the honeycomb cell walls induced by the surface pressure *q*. At the buckling of type *i* cell walls (that is, $\sigma_z = (\sigma_z)_{cr}^{(i)}$), the critical surface pressure $q = q_{cr}^{(i)}$ can be calculated from the following:

$$q_{cr}^{(i)} = \frac{A_w^{(i)}}{A_c^{(i)}}(\sigma_z)_{cr}^{(i)} = \frac{\rho_i}{\rho_c}\frac{(N_z)_{cr}^{(i)}}{t_c} \tag{14}$$

where, for the corrugated cell panel, the panel load $(N_z)_{cr}^{(4)}$ is associated with the unit length along the corrugation length, and for the constant density case ($\rho_4 = \rho_3$), the panel thickness t_c is replaced with $\tilde{t}_c$.

Applying the expressions for the effective densities ρ_i/ρ_c (eqs. (4)–(7)), the buckling pressure $q_{cr}^{(i)}$ associated with type *i* cell can be written as follows:

Type 1:

$$q_{cr}^{(1)} = \frac{16\sqrt{3}}{9d_1}(N_z)_{cr}^{(1)} \tag{15}$$

Type 2:

$$q_{cr}^{(2)} = \frac{2\sqrt{2}}{d_2}(N_z)_{cr}^{(2)} \tag{16}$$

Type 3:

$$q_{cr}^{(3)} = \frac{8\sqrt{2}}{15d_3}\left(\sqrt{2}+3\right)(N_z)_{cr}^{(3)} \tag{17}$$

Type 4:

$$q_{cr}^{(4)} = \frac{8\sqrt{2}}{15d_4}\left(\sqrt{2}+3\sqrt{1+\frac{256}{3}\frac{h_c^2}{d_4^2}}\right)(N_z)_{cr}^{(4)} \tag{18}$$

The panel buckling loads $(N_z)_{cr}^{(1)}, (N_z)_{cr}^{(2)}, (N_z)_{cr}^{(3)}$ for the flat cell wall panels of honeycomb cells types 1, 2, and 3 can be easily calculated from the classical buckling equation for a solid flat rectangular plate (length *a*, width b_i) (ref. 14):

$$(N_z)_{cr}^{(i)} = \frac{\pi^2 D_i}{a^2}\left(m + \frac{n^2}{m}\frac{a^2}{b_i^2}\right)^2 \quad ; \quad i = 1, 2, 3 \tag{19}$$

However, finite-element buckling solutions for the flat cell wall panels of honeycomb cells types 1, 2, and 3 were also obtained and compared with a Timoshenko solution (ref. 14) (eq. (19)). The accuracy of those solutions give confidence in the finite-element buckling solutions obtained for the corrugated panel using similar element density.

For simply supported slender rectangular panels like those with cell wall types 1, 2, and 3, the panels will buckle into several half-waves ($m \neq 1$) in the loading direction, and only one half-wave ($n = 1$) in the transverse direction, (ref. 14). Taking $n = 1$ in equation (19) and minimizing $(N_z)_{cr}^{(i)}$ by differentiating equation (19) with respect to *m*, and then setting the resulting equation to zero, leads to

$$m = \frac{a}{b_i} \tag{20}$$

which gives the correct value of *m* if a/b_i is an integer. If a/b_i is not an integer, the correct value of *m* should be an integer closest to the value of a/b_i.

Alternatively, the value of *m* for minimum buckling load of a rectangular panel with an aspect ratio of a/b_i, can be found graphically from figure 14, the plots of a family of buckling curves associated with different *m* for rectangular plates (ref. 14). Namely, first locate the value of a/b_i on the abscissa, and draw a vertical line from point a/b_i. This vertical line will intersect the curve segment of the lowest buckling load (solid curves, fig. 14), and thereby find the value of *m* associated with that particular buckling curve segment. Table 4 lists the aspect ratios a/b_i and the associated *m* for minimum buckling loads determined for the flat wall panels of types 1, 2, and 3 cells.

Table 4. Aspect ratios and number of buckled half-waves for honeycomb cell wall panels. $\rho_1 = \rho_2 = \rho_3$.

Cell type (*i*)	a/b_i	*m*	*n*
Right hexagonal (*i* = 1)	4.22	4	1
Square (*i* = 2)	3.25	3	1
TPS (flat) (*i* = 3)	3.68	4	1

RESULTS

The effect of honeycomb cell geometry on the heat-shielding performance and cell wall buckling characteristics of a superalloy TPS has been investigated. The results of heat-transfer, thermal bending, and cell wall buckling analyses of superalloy honeycomb TPS panels are presented in the following sections.

Heat Transfer

Figure 15 shows the linear time history of the temperature input to the outer face sheet (point A), and the time histories of the temperatures at the inner face sheet (point B) for different cell geometry. The difference between the outer (T_u; point A) and the inner (T_l; point B) face sheet temperatures, ΔT; $(T_u - T_l)$, is the measure of the heat-shielding performance of the TPS. Namely, the larger the value of ΔT, the better the heat-shielding performance. The ΔT for all cell geometries reaches maximum at approximately 50 sec, then decreases only slightly with the increasing time, *t*. The temperatures at point B for all cell geometries are nearly the same, indicating that the TPS heat-shielding performance is relatively insensitive to the shape change of the honeycomb cell (under the same effective density). The right hexagonal cell has the lowest heat-shielding performance (the lowest ΔT), and the square cell has the highest heat-shielding performance (the highest ΔT). The temperature curves at point B for the two types of TPS cells lie between those for the right hexagonal and square cells. For conduction only (without internal radiation), all the temperature curves at point B for the four types of cell geometry are almost identical, and are hardly distinguishable. The effect of internal radiation turned out to be much smaller than that of conduction for the present TPS core geometry (a = 0.488 in.; d_3 = 0.250 in.). For example, at t = 100 sec (fig. 15), the temperature at point B for the TPS cell (flat wall) consists of 13-percent radiation component and 87-percent conduction component. Table 5 shows typical data of figure 15 at t = 50 sec and t = 100 sec where the "heat-shielding index" is defined as the ratio of ΔT of any cell geometry to the ΔT of the TPS cell with flat cell walls (i = 3) which was used as the reference cell geometry.

Table 5. Heat-shielding performance of superalloy TPS panels with different honeycomb-core cell geometry. $\rho_1 = \rho_2 = \rho_3 = \rho_4 = 0.019976\rho_c$.

	t = 50 sec		t = 100 sec	
Cell type (i)	ΔT, °F	Heat-shielding index	ΔT, °F	Heat-shielding index
Right hexagonal (i = 1)	432	0.99	355	0.95
Square (i = 2)	443	1.02	409	1.09
TPS (h_c = 0) (i = 3)	436	1.00*	375	1.00*
TPS (h_c/t_c = 6) (i = 4)	440	1.01	391	1.04

*Reference cell geometry.

Figure 16 shows the effects of modified core depth a' and cell size d_3 on the heat-shielding performance of TPS with flat cell walls. For the core depth $a' = a$, changing the cell size from $d_3 = 0.25$ in. to $d_3 = 0.5$ in. (reducing effective density) increased ΔT slightly during the initial heating stage until $t = 65$ sec, but reduced ΔT after $t = 65$ sec. For the deeper core depths ($a' = 1.5a$ and $a' = 2a$), the honeycomb core with the smaller cell size ($d_3 = 0.25$ in.) has better heat-shielding performance (larger ΔT) than those with the larger cell size ($d_3 = 0.5$ in.), which have lower effective density. The comparatively lower values of ΔT for the larger cell size $d_3 = 0.5$ in. is caused by the increased radiation effect from the upper face sheet to the lower face sheet. Table 6 shows typical data from figure 16 at t = 50 sec and t = 100 sec, where the "weight index" is defined as the ratio of the weight of an $l \times l$ TPS panel with any cell size d_3 and depth a' to the weight of an $l \times l$ TPS panel with cell size $d_3 = 0.25$ in. and depth $a' = a = 0.488$ in. calculated using equation (3).

Table 6. Heat shielding performance of TPS honeycomb-core with different cell sizes and core depths; flat cell walls ($i = 3$).

		t = 50 sec		t = 100 sec		
Cell size (d_3), in.	a', in.	ΔT	Heat-shielding index	ΔT	Heat-shielding index	Weight index
0.250	0.488 (1a)	436	1.00*	375	1.00*	1.00*
0.250	0.732 (1.5a)	592	1.36	633	1.69	1.25
0.250	0.976 (2a)	682	1.56	886	2.36	1.50
0.375	0.488 (1a)	455	1.04	321	0.86	0.83
0.375	0.732 (1.5a)	592	1.36	531	1.42	1.00
0.375	0.976 (2a)	674	1.55	754	2.01	1.17
0.500	0.488 (1a)	466	1.07	284	0.76	0.75
0.500	0.732 (1.5a)	587	1.35	454	1.21	0.87
0.500	0.976 (2a)	664	1.52	642	1.71	1.00

*Reference cell geometry.

Thermal Bending

Figures 17 and 18 respectively show typical deformed shapes of honeycomb TPS panel subjected to thermal bending (T_u = 800 °F; T_l = 450 °F) for cases with simply supported fixed corners and simply supported fixed edges. Table 7 shows a summary of the deflections at the sandwich panel edge midpoint, w_e, and center, w_{max}, and stresses $\{\sigma_x, \sigma_y\}$ induced at the centers of the upper and lower face sheets.

Note that only for the "free simply supported corners" case (marked with an asterisk in table 7) are the face sheets stress-free; however, the TPS panel bulged out 0.4144 in. To eliminate TPS outward bulging, the panel support condition must be either "fixed clamped edges" or "free clamped edges" (marked with a dagger in table 7). These two support conditions, however, will certainly induce higher stresses in the face sheets. The simply supported and clamped fixed edge cases induced extremely high face sheet stresses that could cause the entire TPS panel to buckle (ref. 15).

Table 7. Panel deflections and thermal stresses induced in the face sheets of superalloy honeycomb TPS under different support conditions; T_u = 800 °F; T_l = 450 °F; TPS cell (flat walls, i = 3).

	Panel center	Edge midpoint	Upper center		Lower center	
Boundary condition	w_{max}, in.	w_e, in.	σ_x, lb/in^2	σ_y, lb/in^2	σ_x, lb/in^2	σ_y, lb/in^2
Fixed simply supported corners	0.4144	0.2061	–25,060	–25,060	–25,060	–25,060
Free simply supported corners*	0.4144	0.2061	0	0	0	0
Fixed clamped corners	0.2926	0.1085	–33,820	–33,870	–16,300	–16,240
Free clamped corners	0.2926	0.1085	–8,760	–8,820	8,760	8,820
Fixed simply supported edges	0.1689	0	–201,420	–201,360	–166,340	–166,410
Free simply supported edges	0.1689	0	–17,540	–17,480	17,540	17,480
Fixed clamped edges†	0	0	–241,390	–241,390	–126,370	–126,370
Free clamped edges†	0	0	–57,510	–57,510	57,510	57,510

*Support condition for stress-free face sheets.
†Support conditions for zero TPS panel deflection.

Cell Wall Buckling

Figure 19 shows buckling shapes of the four types of honeycomb cell wall panels under axial compression caused by air load. As predicted in table 4, the right hexagonal cell wall and the TPS cell flat wall buckled into four half-waves in the cell axial direction (figs. 19(a) and 19(c)). The square cell wall panel buckled into three half-waves (fig. 19(b)) in the cell axial direction; and the TPS cell corrugated wall ($h_c/t_c = 6$) buckled into only one half-wave in the cell axial direction because of corrugation (fig. 19(d)). Table 8 shows a summary of the numerical results of honeycomb cell wall buckling analysis, and that the buckling solutions obtained from the SPAR finite-element method and Timoshenko classical elasticity theory (ref. 14) are extremely close, giving confidence in the accuracy of the SPAR buckling solution obtained for the corrugated cell wall case ($i = 4$).

Table 8. Buckling pressures of superalloy honeycomb TPS with different cell geometry.

Cell type (i)	$q_{cr}^{(i)}$, lb/in^2		Solution difference, percent	$q_{cr}^{(i)}/q_{cr}^{(3)}$
	Timoshenko	SPAR		
Right hexagonal ($i = 1$)	214.7460	214.8327	0.0404	1.31
Square ($i = 2$)	127.7003	127.7508	0.0395	0.78
TPS ($h_c = 0$) ($i = 3$)	163.9307	164.1705	0.1463	1.00*
TPS ($h_c/t_c = 6$) ($i = 4$)	No theory	682.0951	N/A	4.16

*Reference cell geometry.

As shown earlier, the heat-shielding performances of different types of honeycomb cells are quite similar. The air pressure buckling strengths, however, are quite different (table 8). The cell axial buckling strengths of the right hexagonal and square cells respectively are 1.31 and 0.78 times that of the TPS cell with flat walls. The TPS cell with corrugated walls ($h_c/t_c = 6$) has a buckling strength 4.16 times that of the TPS cell with flat walls ($h_c = 0$).

The maximum dynamic pressure a Space Shuttle orbiter has experienced during reentry is approximately 1.84 lb/in^2 (265 lb/ft^2) at Mach 0.6. Considering that the new STS will be subjected to similar dynamic pressure, these four types of honeycomb cells certainly have excess buckling strengths to carry the surface air load.

Figure 20 shows plots of buckling pressure $q_{cr}^{(i)}$ and core density ρ_i/ρ_c of type i cells as functions of honeycomb cell size d_i. This figure provides vital design curves for the honeycomb cells. Figure 20 is used as follows: for a given fixed core density $\rho_i/\rho_c = 0.019976$, a horizontal line ABC is drawn to intersect the core density curves ρ_3, ρ_1, and ρ_2 for cell types 3, 1, and 2. Then vertical lines are drawn from points A, B, and C. The intersection of those vertical lines with the abscissa then gives the cell sizes $d_3 = 0.25$ in., $d_1 = 0.2312$ in., and

d_2 = 0.2124 in. The intersections of the vertical lines drawn from points A, B, and C with the $q_{cr}^{(i)}$ curves give the values of buckling pressure $q_{cr}^{(i)}$ associated with each cell type; namely, $q_{cr}^{(3)}$ = 163.93 lb/in^2, $q_{cr}^{(1)}$ = 214.75 lb/in^2, and $q_{cr}^{(2)}$ = 127.70 lb/in^2. Note that the right hexagonal cell has the highest buckling strength, and the square cell has the lowest buckling strength. The value of buckling pressure of the TPS cell with flat walls ($q_{cr}^{(3)}$) lies between those of the right hexagonal cell and square cell (table 8).

Figure 21 shows the plots of buckling pressure $q_{cr}^{(4)}/q_{cr}^{(3)}$, core density ρ_4/ρ_3, and sandwich density $\rho_{sw}^{(4)}/\rho_{sw}^{(3)}$ of TPS cells with corrugated walls as functions of the corrugation depth h_c/t_c. Data for plotting the curves associated with this cell are normalized by the corresponding values associated with the TPS cell with flat walls (type 3 cell). Figure 21 shows two cases of buckling curves. The first case has a constant sandwich density (that is, $\rho_{sw}^{(4)} = \rho_{sw}^{(3)}$), but $\tilde{t}_c$ is a function of corrugation depth h_c/t_c. The second case has a constant corrugation wall thickness (that is, $\tilde{t}_c = t_c$), but the core density ρ_4/ρ_3 and the sandwich density $\rho_{sw}^{(4)}/\rho_{sw}^{(3)}$ can change with the corrugation depth h_c/t_c.

At the lower value of h_c/t_c ($h_c/t_c \le 0.5$), the corrugated panel behaved like the flat wall panel (table 4) and buckled into four half-waves (m = 4, n = 1) in the cell axis direction. The corrugated panel then buckled into (m = 3, n = 1) mode in the region $0.5 < (h_c/t_c) < 2$, and then into (m = 2, n = 1) mode in the region $2 < h_c/t_c < 5.5$, and finally into (m = 1, n = 1) mode when the corrugation depth h_c/t_c was increased beyond h_c/t_c = 5.5.

Buckling pressure $q_{cr}^{(4)}/q_{cr}^{(3)}$ of the second case (t_c = constant) is slightly higher (by 1.83 percent at h_c/t_c = 6) than that of the first case because in the first case, the cell wall thickness $\tilde{t}_c$ decreased with the increasing corrugation depth h_c/t_c and thus lowered the buckling pressure. By keeping the wall thickness constant, $\tilde{t}_c = t_c$, independent of the corrugation depth change (case 2), the honeycomb core density ρ_4/ρ_3 and sandwich panel density $\rho_{sw}^{(4)}/\rho_{sw}^{(3)}$ increased by merely 3.66 and 1.64 percent, respectively, at h_c/t_c = 6. These amounts of density sacrifices could be considered insignificant.

CONCLUSIONS

Heat-transfer, thermal bending, and mechanical buckling analyses were performed on a superalloy thermal protection system (TPS) for future hypersonic flight vehicles. Effect of honeycomb cell geometry on the heat-shielding performance and honeycomb cell wall buckling characteristics, and the effect of boundary conditions on the TPS thermal bending, were investigated.

The results are summarized as follows:

1. The heat-shielding performance of a honeycomb TPS is insensitive to the shape of the honeycomb cell under the same effective core density, but improves with the core depth.
2. The TPS outward bulging effect can be eliminated if the panel support condition is either “fixed clamped edges” or “free clamped edges.” The latter case is preferred because of much lower stresses.
3. To reduce the TPS face sheet stresses to zero, the boundary support condition must be “free simply supported corners.”

4. The cell axial buckling strength is somewhat sensitive to the shape of honeycomb cell, but is quite sensitive to the depth of cell wall corrugation. The right hexagonal cell and square cell have axial buckling strengths 1.31 and 0.78 times, respectively, that of the TPS cell with flat walls; and the TPS cell with corrugated walls with corrugation depth $h_c / t_c = 6$ has buckling strength 4.16 times that of the TPS cell with flat walls.
5. Through corrugation of the honeycomb cell walls, the buckling pressure of the TPS panel could be enhanced greatly.

Dryden Flight Research Center
National Aeronautics and Space Administration
Edwards, California
March 1, 2001

FIGURES

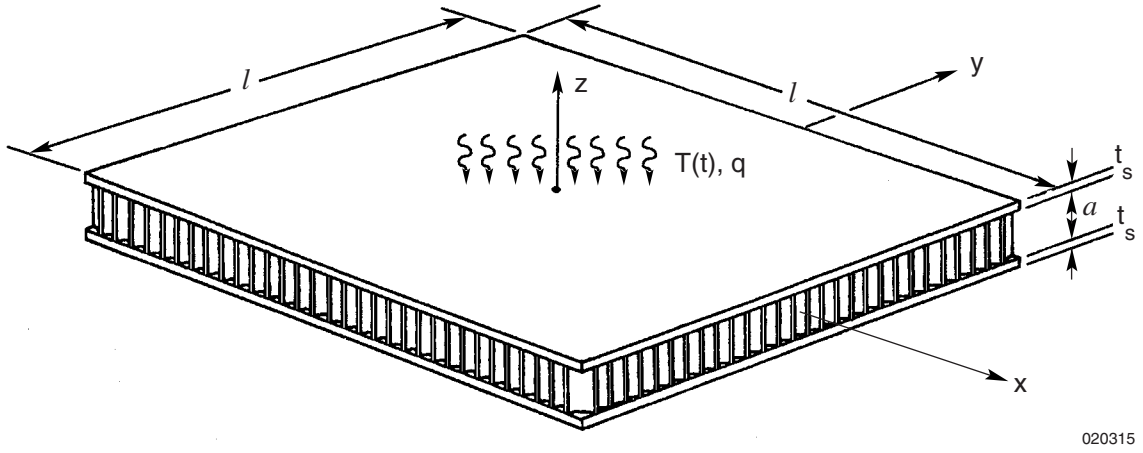

Figure 1. Honeycomb sandwich thermal protection system (TPS) subjected to heating *T(t)* and aerodynamic pressure *q* over entire upper surface.

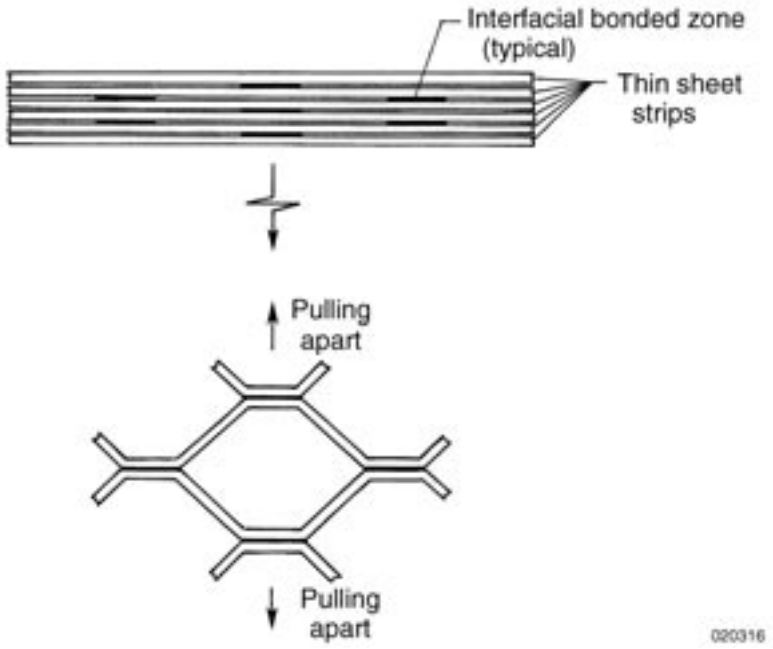

Figure 2. Formation of honeycomb structure through pulling apart of joined thin strip foil assembly.

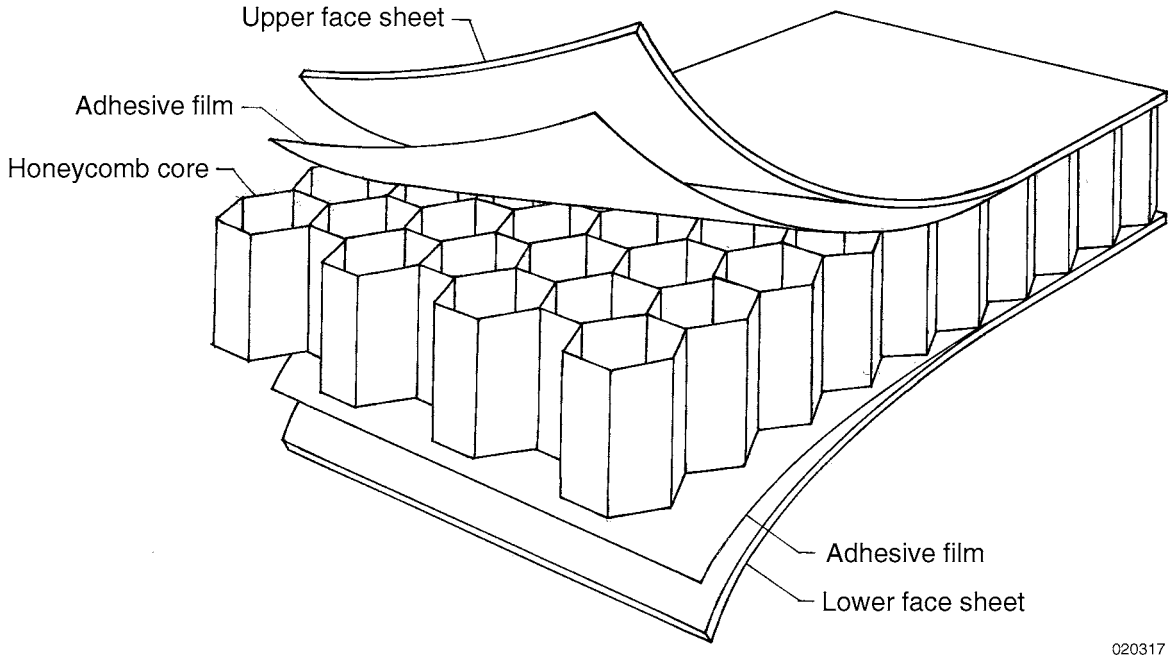

Figure 3. Exploded view of honeycomb core sandwich panel.

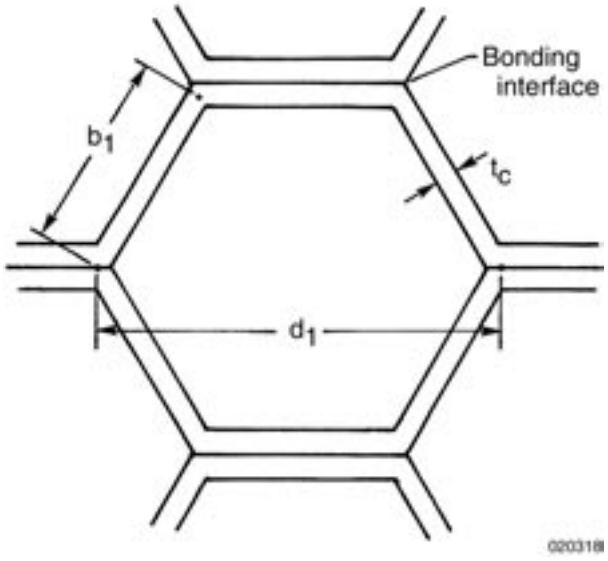

(a) Right hexagonal cell.

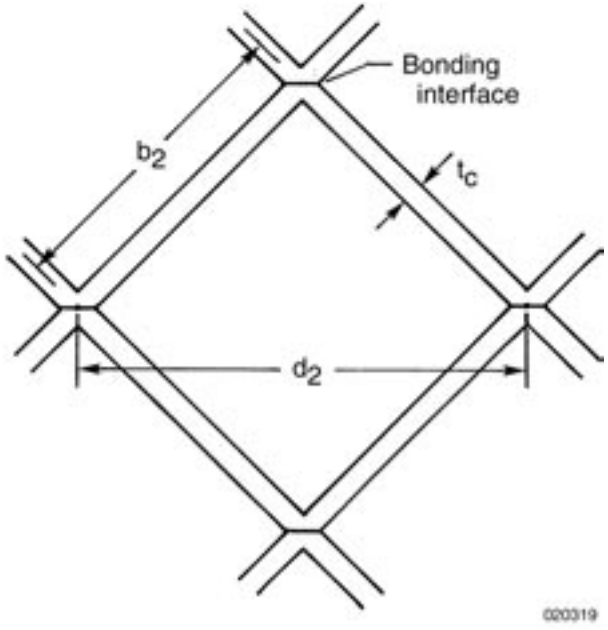

(b) Square cell.

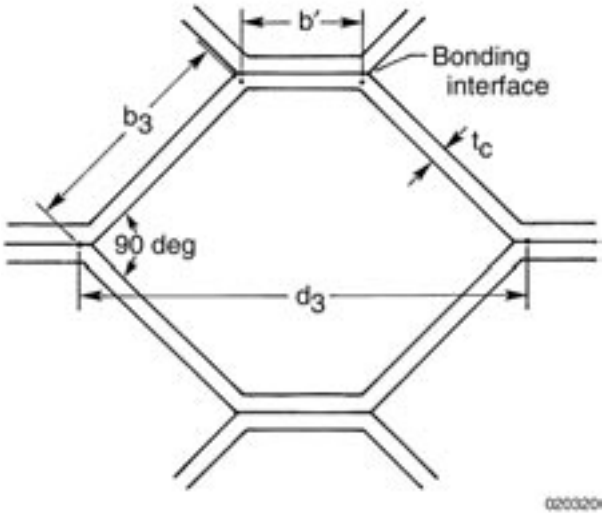

(c) TPS cell (flat walls).

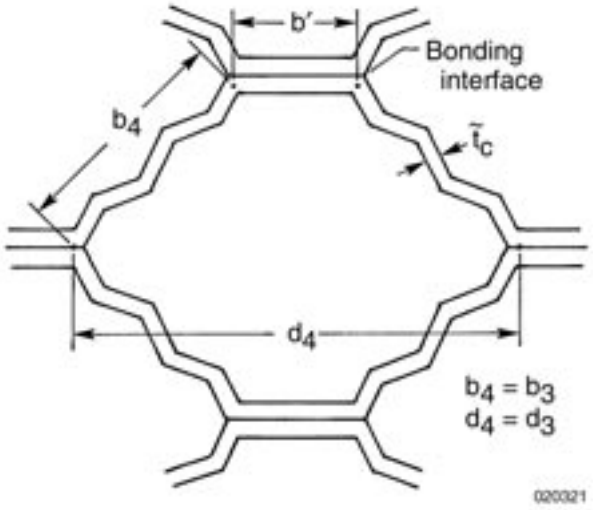

(d) TPS cell (corrugated walls).

Figure 4. Four types of honeycomb cell geometries.

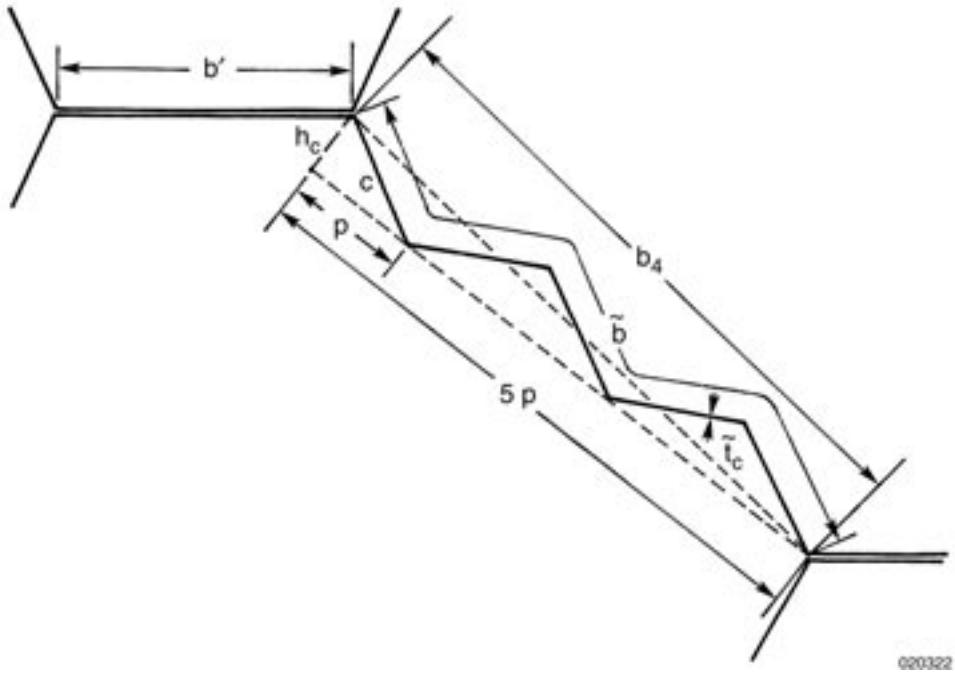

Figure 5. Detailed geometry of TPS cell corrugated wall.

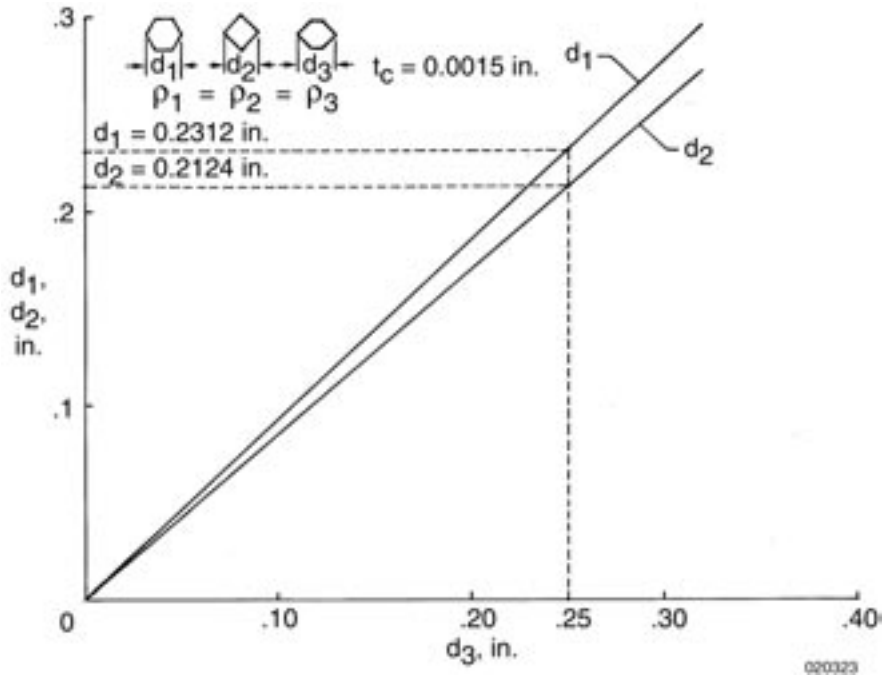

Figure 6. Relationships between the cell sizes d_i of different honeycomb cells having identical core densities; $\rho_1 = \rho_2 = \rho_3$.

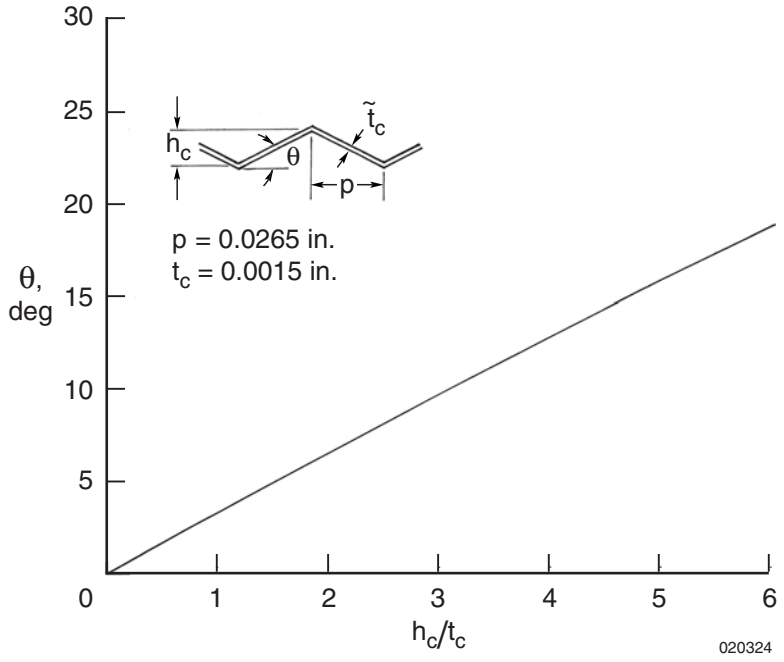

Figure 7. Relationship between TPS cell wall corrugation angle, θ, and corrugation depth h_c/t_c.

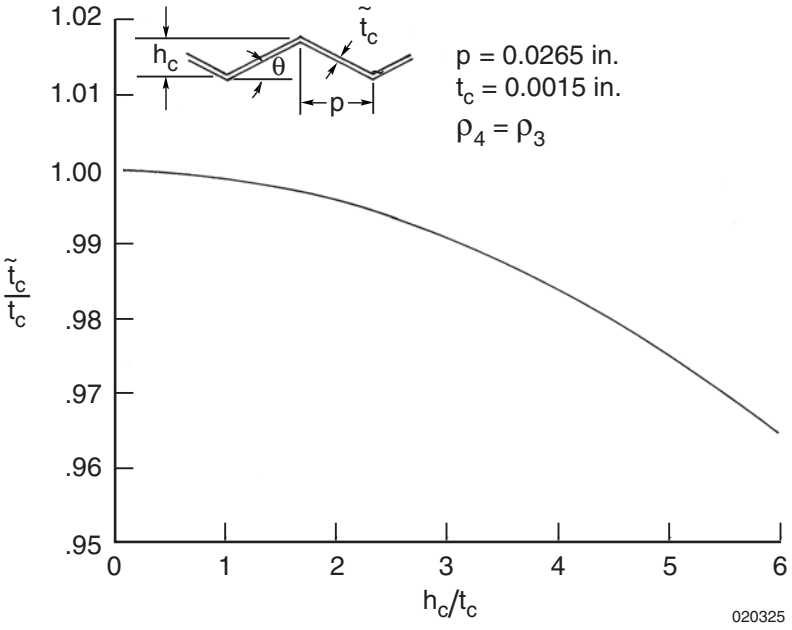

Figure 8. Decreasing of TPS cell corrugated wall thickness $\tilde{t}_c/t_c$ with the increasing corrugation depth h_c/t_c under constant core density; $\rho_4 = \rho_3$.

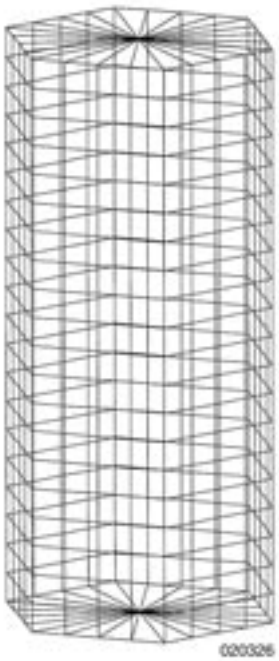

(a) Right hexagonal cell.

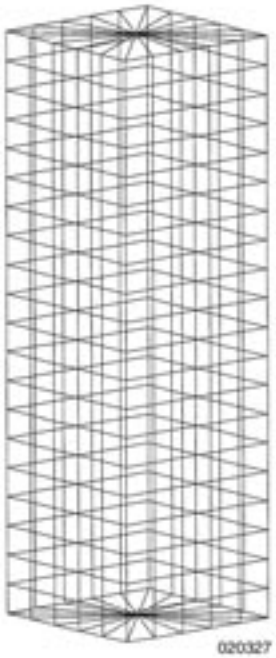

(b) Square cell.

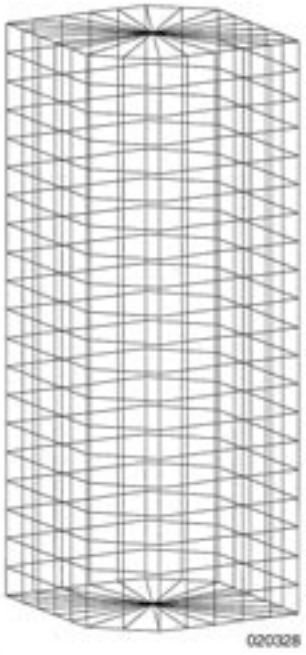

(c) TPS cell (flat walls).

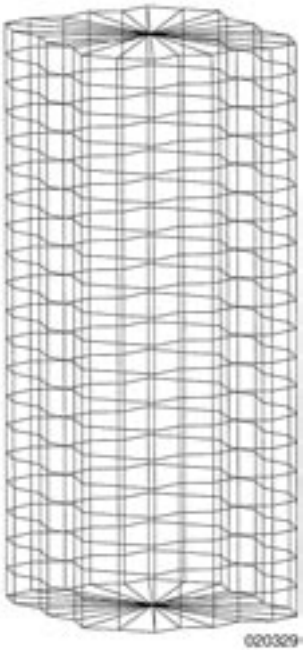

(d) TPS cell (corrugated walls).

Figure 9. Finite-element models for different unit honeycomb cells for heat transfer analysis.

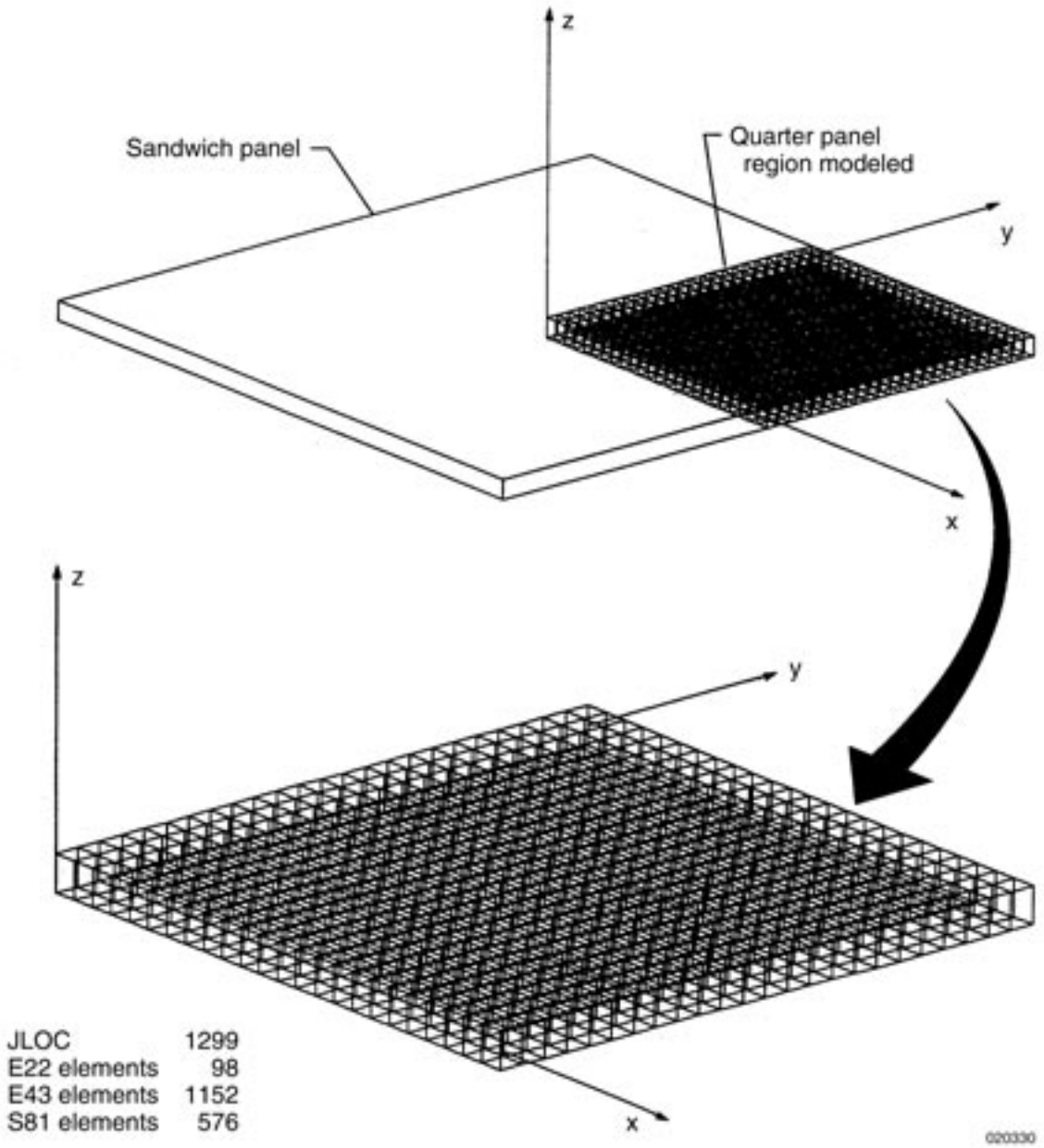

Figure 10. Quarter-panel finite-element model for honeycomb sandwich TPS panel for thermal bending analysis.

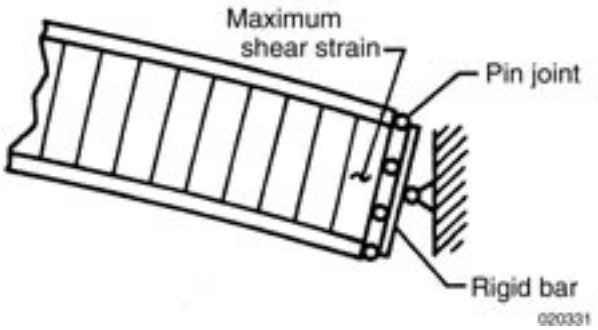

(a) Fixed simply supported edge or corner.

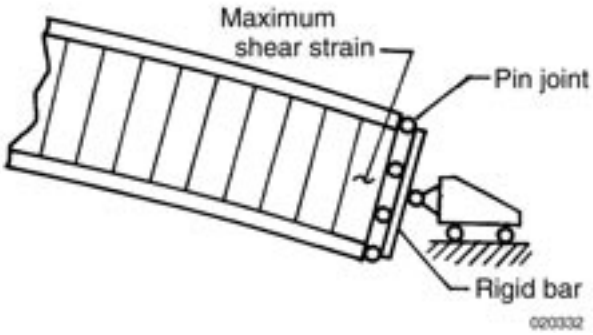

(b) Free simply supported edge or corner.

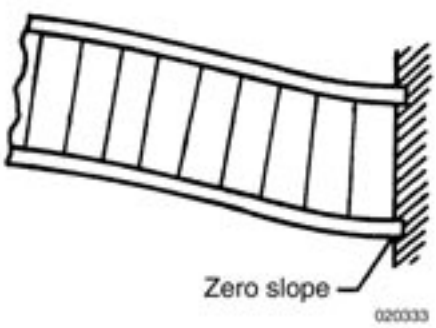

(c) Fixed clamped edge or corner.

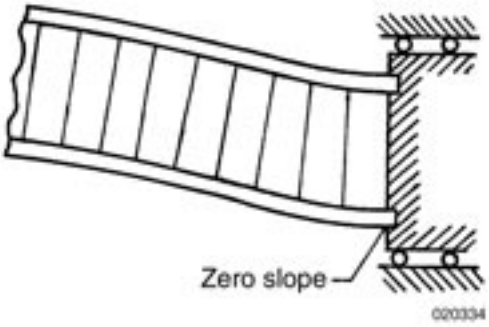

(d) Free clamped edge or corner.

Figure 11. Different support conditions at edges or corners of honeycomb sandwich TPS panel.

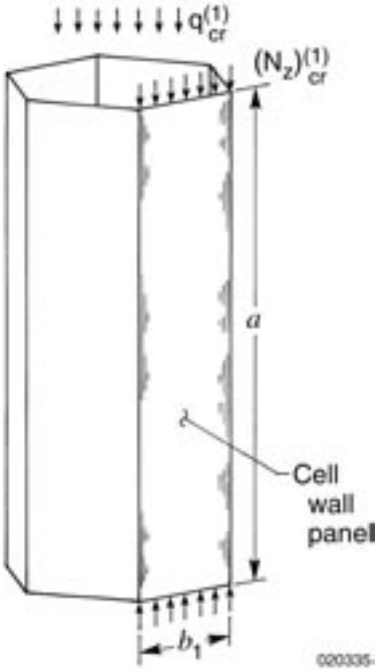

(a) Right hexagonal cell wall panel.

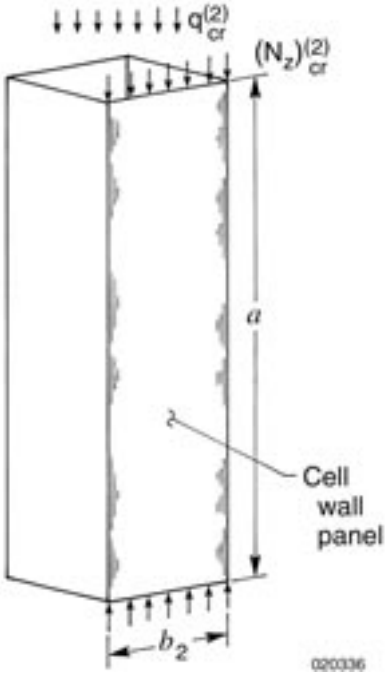

(b) Square cell wall panel.

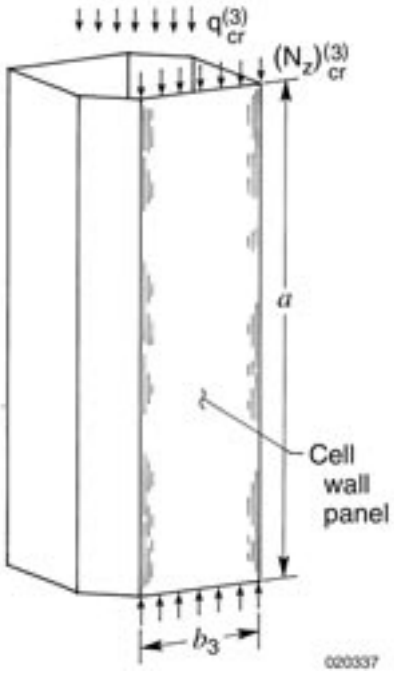

(c) TPS cell flat wall panel.

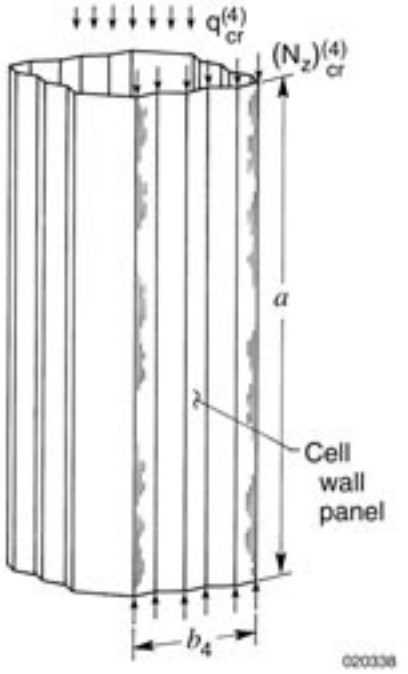

(d) TPS cell corrugated wall panel.

Figure 12. Different honeycomb unit cell wall panels for compressive buckling analysis.

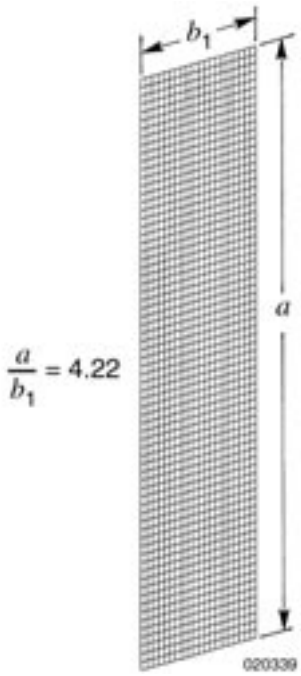

(a) Right hexagonal cell wall panel.

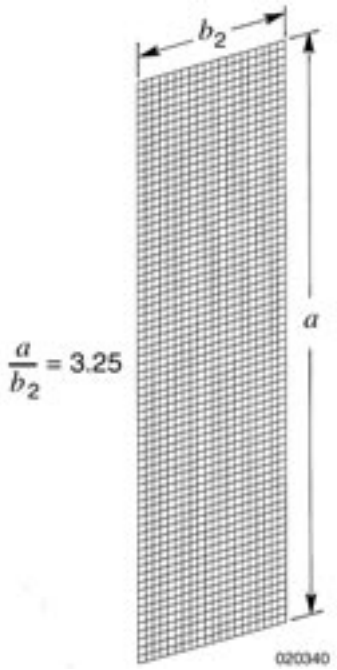

(b) Square cell wall panel.

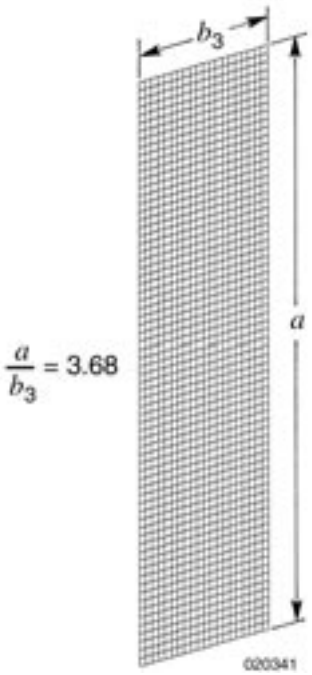

(c) TPS cell flat wall panel.

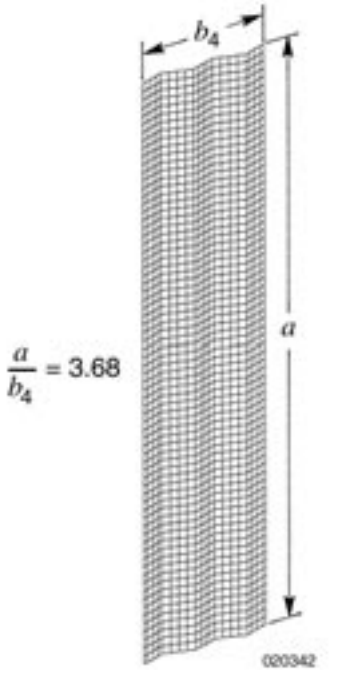

(d) TPS cell corrugated wall panel.

Figure 13. Finite-element models for different honeycomb cell wall panels for compressive buckling analysis.

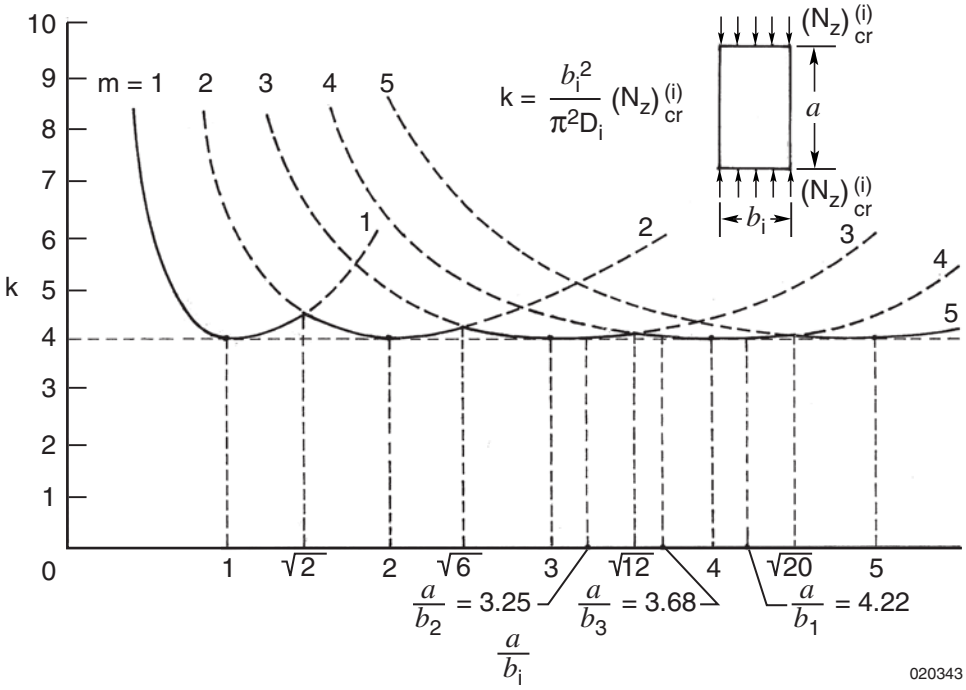

Figure 14. Buckling curves for rectangular plates with different aspect ratios a/b_i (ref. 14).

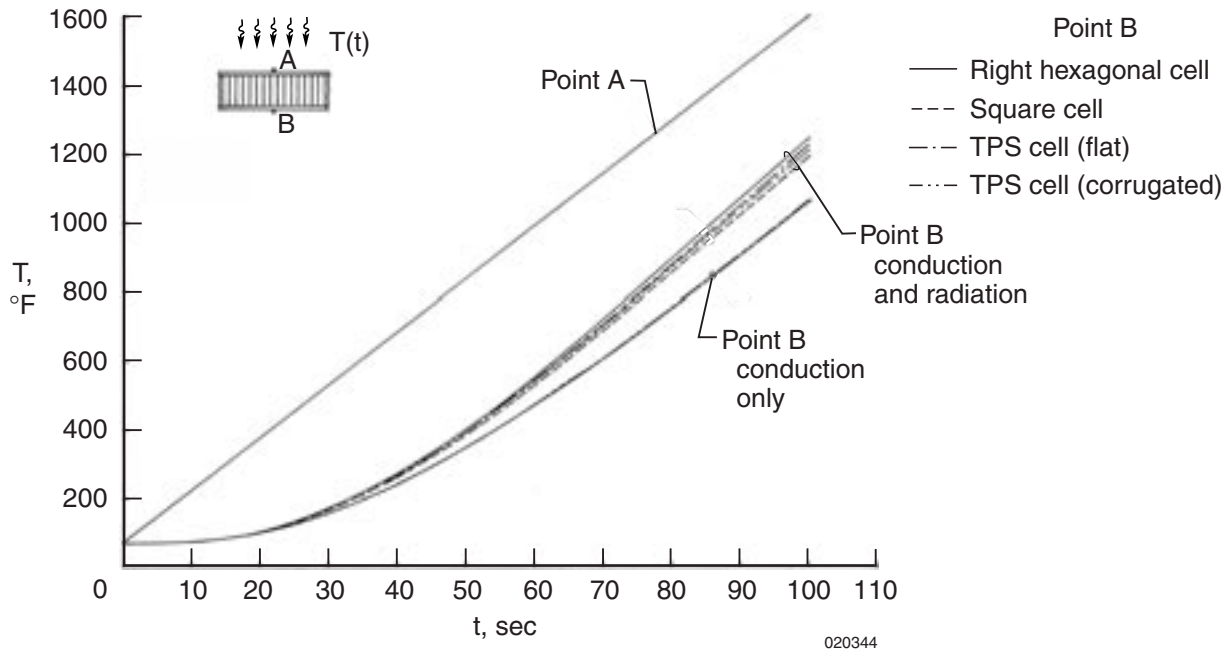

Figure 15. Effect of honeycomb cell geometry on the heat-shielding performance of superalloy honeycomb TPS panel.

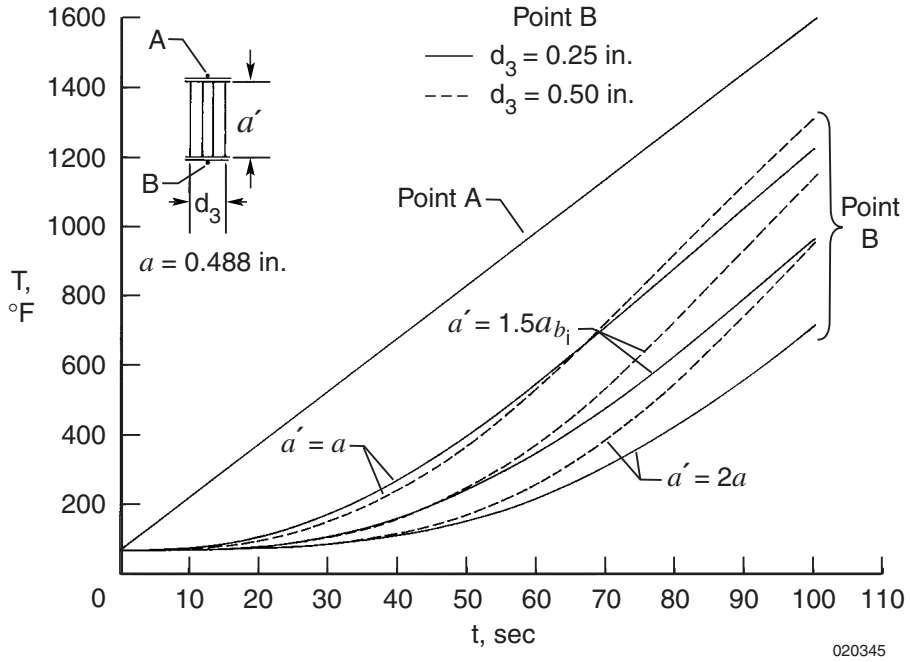

Figure 16. Effects of cell sizes and core depths on the heat-shielding performance of superalloy honeycomb TPS panel; TPS cell with flat cell walls.

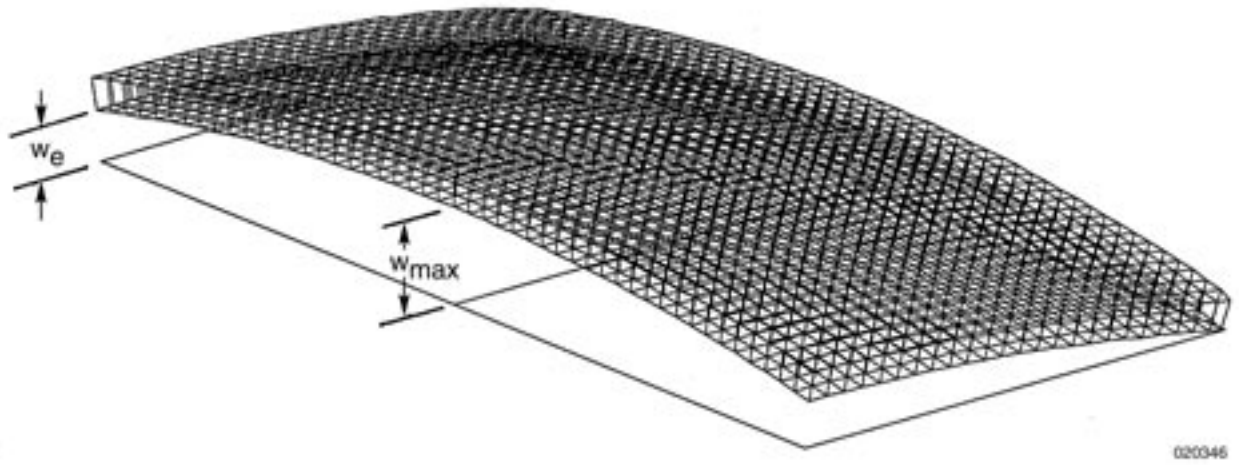

Figure 17. Deformed shape of honeycomb sandwich TPS panel under differential surface heating; T_u = 800 °F, T_l = 450 °F; simply supported fixed corners.

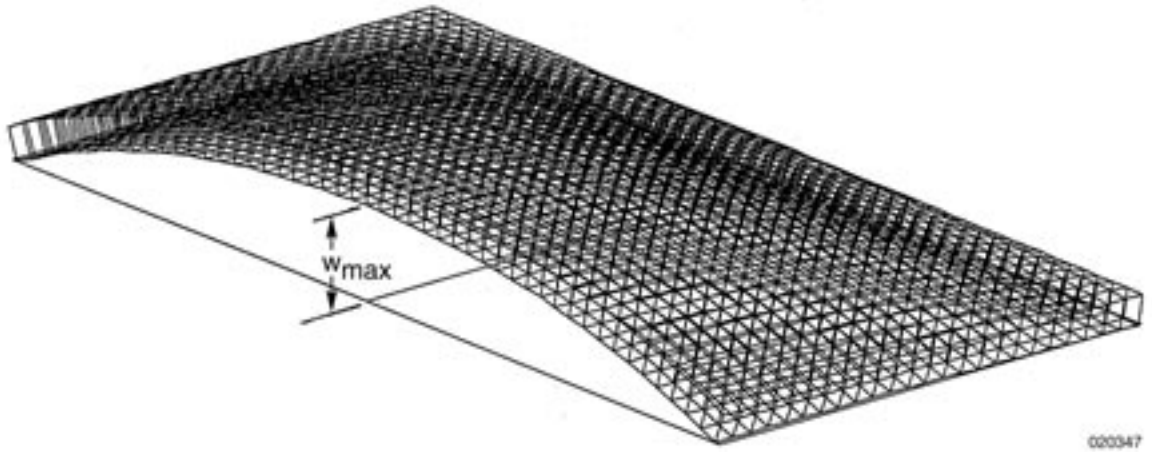

Figure 18. Deformed shape of honeycomb sandwich TPS panel under differential surface heating; T_u = 800 °F, T_l = 450 °F; simply supported fixed edges.

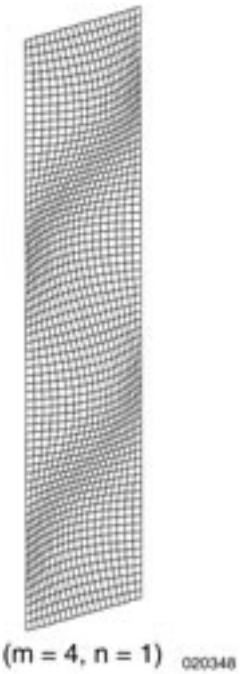

(a) Right hexagonal cell wall panel.

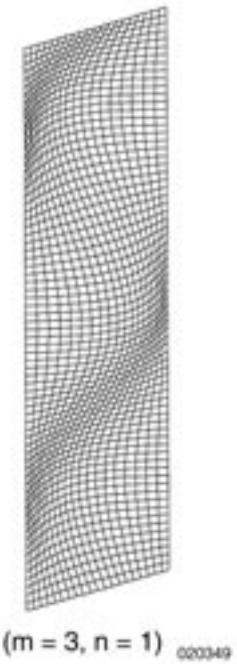

(b) Square cell wall panel.

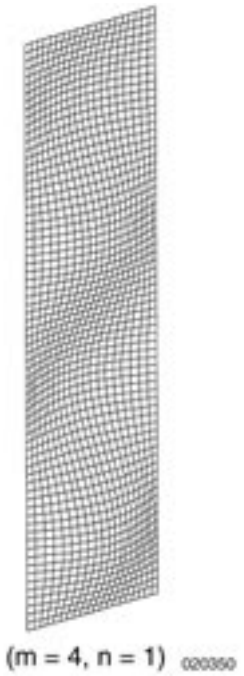

(c) TPS cell flat wall panel.

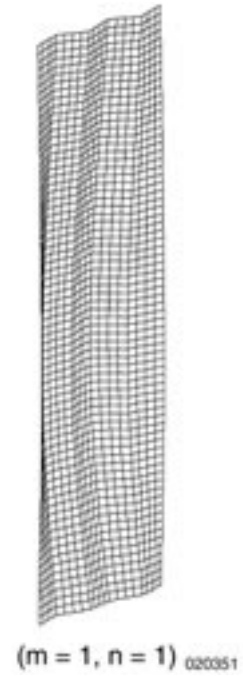

(d) TPS cell corrugated wall panel.

Figure 19. Buckled shapes of different honeycomb cell wall panels; simply supported.

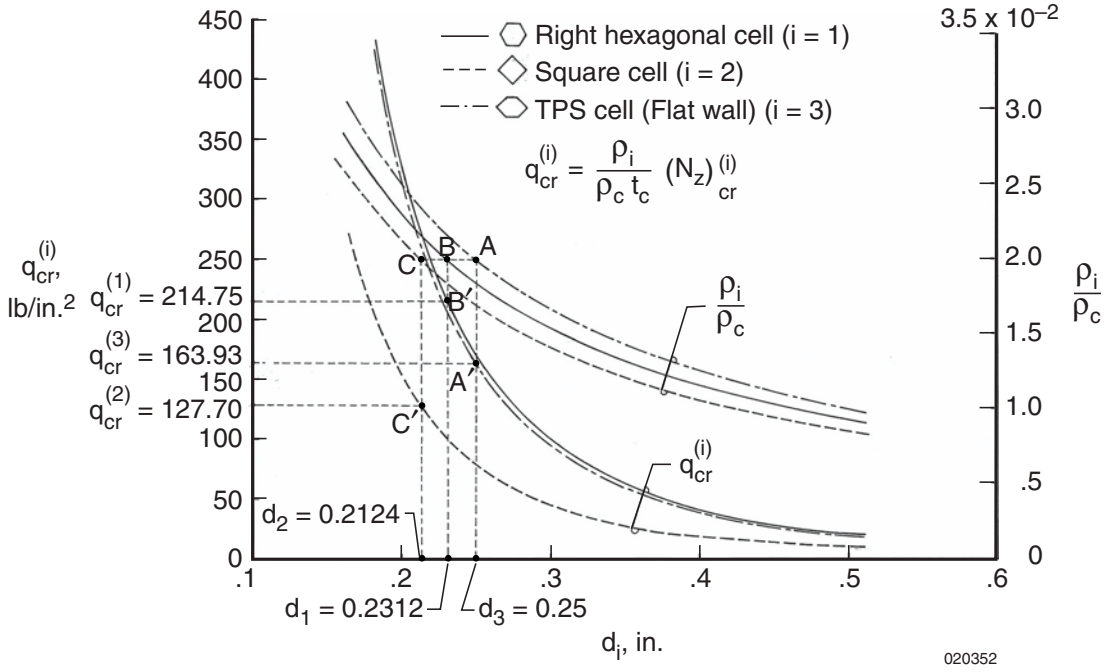

Figure 20. Plots of buckling pressure $q_{cr}^{(i)}$ and core densities ρ_i/ρ_c as functions of honeycomb cell size d_i.

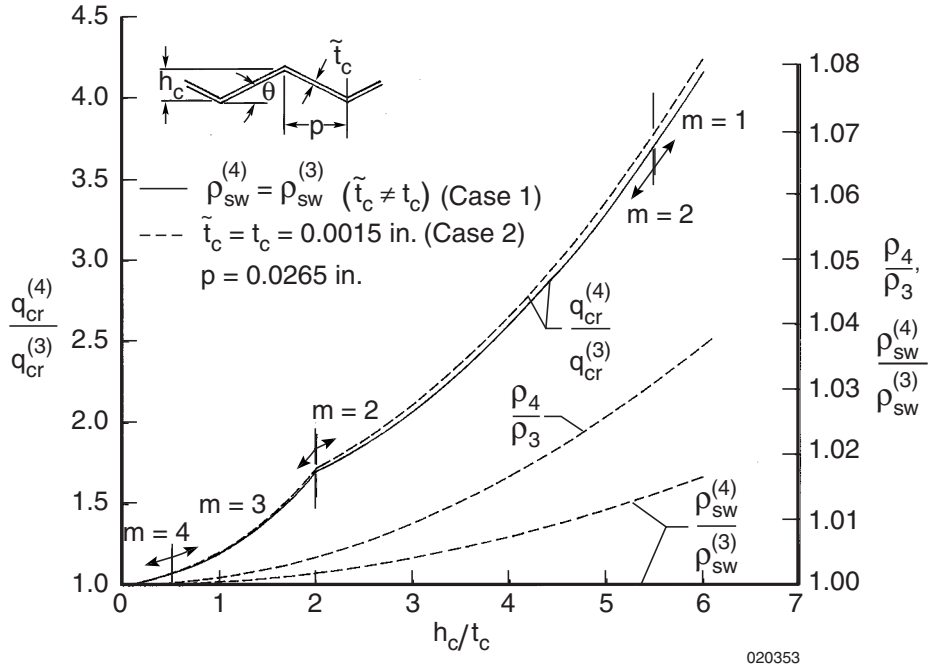

Figure 21. Plots of buckling pressure $q_{cr}^{(4)}/q_{cr}^{(3)}$ and core density ρ_4/ρ_3 of corrugated TPS cell as functions of corrugation depth h_c/t_c.

APPENDIX

HONEYCOMB CELL ANALYSIS

The geometrical analyses of the four types of honeycomb cells are performed below. In each honeycomb cell are two interbonded double cell walls of thickness $2t_c$ (interbonded region diminished theoretically for the square cell), and four free cell walls with single thickness t_c. In the calculations of the wall cross-sectional area $A_w^{(i)}$ of the unit cell, only one-half of cell wall thickness is used because each cell wall panel is mutually shared by two adjacent cells. Namely, for the free cell walls, thickness $t_c/2$ is used; and for the bonded double walls, thickness $2t_c/2 = t_c$ is used.

Right Hexagonal Cell:

From figure 3(a), the length b_1 of one side of the right hexagon is related to the cell size d_1 through

$$b_1 = \frac{d_1}{2} \tag{A-1}$$

The cross-sectional area $A_c^{(1)}$ of the unit right hexagonal cell (consisting of six right triangles) can be calculated as

$$A_c^{(1)} = 6\left(\frac{b_1}{2}\right)\left(\frac{\sqrt{3}}{2}b_1\right) = \frac{3\sqrt{3}}{2}b_1^2 \tag{A-2}$$

The cross-sectional area $A_w^{(1)}$ of the unit hexagonal cell wall, which consists of two bonded sides and four free sides, can be calculated as follows:

$$A_w^{(1)} = 2b_1\left(\frac{2t_c}{2}\right) + 4b_1\left(\frac{t_c}{2}\right) = 4b_1t_c \tag{A-3}$$

From equation (A-2) and (A-3), the effective density ρ_1 of the right hexagonal cell can be expressed as

$$\frac{\rho_1}{\rho_c} = \frac{A_w^{(1)}}{A_c^{(1)}} = \frac{8\sqrt{3}t_c}{9b_1} = \frac{16\sqrt{3}t_c}{9d_1} \;;\; b_1 = \frac{d_1}{2} \tag{A-4}$$

Square Cell:

From figure 3(b), the length b_2 of one side of the square cell is related to the cell size d_2 as

$$b_2 = \frac{\sqrt{2}d_2}{2} \tag{A-5}$$

The cross-sectional area $A_c^{(2)}$ of the unit square cell is given by

$$A_c^{(2)} = b_2^2 \tag{A-6}$$

The cross-sectional area $A_w^{(2)}$ of the square cell wall (consisting of four free sides) is expressed as

$$A_w^{(2)} = 4b_2\left(\frac{t_c}{2}\right) = 2b_2t_c \tag{A-7}$$

In light of equations (A-6) and (A-7), the effective density ρ_2 of the square cell is given by

$$\frac{\rho_2}{\rho_c} = 2\frac{t_c}{b_2} = 2\sqrt{2}\frac{t_c}{d_2} \;\; ; \;\; b_2 = \frac{\sqrt{2}d_2}{2} \tag{A-8}$$

TPS Cell (Flat Wall):

From figure 3(c), the length b_3 and b' are respectively related to the cell size d_3 as

$$b_3 = \frac{3\sqrt{2}}{8}d_3 \;\; ; \;\; b' = \frac{d_3}{4} = \frac{\sqrt{2}}{3}b_3 \tag{A-9}$$

The cross-sectional area $A_c^{(3)}$ of the unit TPS cell (consisting of two identical trapezoids) can be calculated as

$$A_c^{(3)} = 2\left[\frac{1}{2}\left(d_3 + b'\right)\frac{b_3}{\sqrt{2}}\right] = \frac{5}{3}b_3^2 \tag{A-10}$$

in which equation (A-9) was applied. And, the cross-sectional area $A_w^{(3)}$ of the unit TPS cell wall (consisting of four free sides and two bonded sides) can be calculated as

$$A_w^{(3)} = 4b_3\left(\frac{t_c}{2}\right) + 2b'\left(\frac{2t_c}{2}\right) = 2(b_3 + b')t_c \tag{A-11}$$

which becomes, in light of equation (A-9),

$$A_w^{(3)} = \frac{2}{3}\left(3 + \sqrt{2}\right)b_3t_c \tag{A-12}$$

From equations (A-10) and (A-12), the effective density ρ_3 of the TPS cell (flat wall) can be expressed as

$$\frac{\rho_3}{\rho_c} = \frac{A_w^{(3)}}{A_c^{(3)}} = \frac{2}{5}\left(3+\sqrt{2}\right)\frac{t_c}{b_3} = \frac{8\sqrt{2}}{15}\left(3+\sqrt{2}\right)\frac{t_c}{d_3} \;\; ; \;\; b_3 = \frac{3\sqrt{2}}{8}d_3 \tag{A-13}$$

TPS Cell (Corrugated Wall):

From figure 3(d), the length b_4 and b' are respectively related to the cell size d_4 as

$$b_4 = \frac{3\sqrt{2}}{8}d_4 \;\; ; \;\; b' = \frac{d_4}{4} = \frac{\sqrt{2}}{3}b_4 \tag{A-14}$$

Considering equation (A-9), the cross-sectional area $A_c^{(4)}$ of the unit TPS cell (consisting of two identical trapezoids) can be calculated as

$$A_c^{(4)} = 2\left[\frac{1}{2}\left(d_4 + b'\right)\frac{b_4}{\sqrt{2}}\right] = \frac{5}{3}b_4^2 \tag{A-15}$$

And, the cross-sectional area $A_w^{(4)}$ of the unit TPS cell wall (consisting of four free sides and two double sides) can be calculated as follows:

$$A_w^{(4)} = 4\tilde{b}\left(\frac{\tilde{t}_c}{2}\right) + 2b'\left(\frac{2\tilde{t}_c}{2}\right) = 2\left(\tilde{b} + b'\right)\tilde{t}_c \tag{A-16}$$

which becomes, in light of equation (A-14),

$$A_w^{(4)} = 2\left(\tilde{b} + \frac{\sqrt{2}}{3}b_4\right)\tilde{t}_c \tag{A-17}$$

From equations (A-15) and (A-17), the effective density ρ_4 of the TPS cell (corrugated wall) can be expressed as

$$\frac{\rho_4}{\rho_c} = \frac{A_w^{(4)}}{A_c^{(4)}} = \frac{2}{5}\left(3\frac{\tilde{b}}{b_4} + \sqrt{2}\right)\frac{\tilde{t}_c}{b_4} \tag{A-18}$$

where the corrugated side length $\tilde{b}$ is calculated in the following.

The TPS cell with corrugated wall (fig. 3(d)) has identical size and cell density as the TPS cell with flat wall (fig. 3(c)). Therefore, to maintain constant effective density $\rho_4 = \rho_3$, the corrugated wall thickness $\tilde{t}_c$ must be

modified whenever the corrugation depth h_c is changed. From figure 4, the corrugation true length $\tilde{b}$ consists of five identical corrugation legs of length *c*. Namely,

$$\tilde{b} = 5c \tag{A-19}$$

The length *c* of each corrugation leg is related to the corrugation half-pitch *p* and the corrugation depth h_c through

$$c = \sqrt{p^2 + h_c^2} \tag{A-20}$$

where the half-pitch length *p* is related to b_4 (end-to-end distance of corrugation side (fig. 4)) and h_c through

$$5p = \sqrt{b_4^2 - h_c^2} \tag{A-21}$$

Combining the above three equations results in

$$\frac{\tilde{b}}{b_4} = \sqrt{1 + 24\frac{h_c^2}{b_4^2}} = \sqrt{1 + \frac{256}{3}\frac{h_c^2}{d_4^2}} \quad ; \quad b_4 = \frac{3\sqrt{2}}{8}d_4 \tag{A-22}$$

Substituting equation (A-22) into equation (A-18) yields

$$\frac{\rho_4}{\rho_c} = \frac{A_w^{(4)}}{A_c^{(4)}} = \frac{2}{5}\left(3\sqrt{1 + 24\frac{h_c^2}{b_4^2}} + \sqrt{2}\right)\frac{\tilde{t}_c}{b_4} = \frac{8\sqrt{2}}{15}\left(3\sqrt{1 + \frac{256}{3}\frac{h_c^2}{d_4^2}} + \sqrt{2}\right)\frac{\tilde{t}_c}{d_4} \quad ; \quad b_4 = \frac{3\sqrt{2}}{8}d_4 \tag{A-23}$$

For the constant effective density ($\rho_4 = \rho_3$) (that is, $A_w^{(4)} = A_w^{(3)}$), the corrugated cell wall thickness $\tilde{t}_c$ is related to t_c through

$$2\left(\tilde{b} + b'\right)\tilde{t}_c = 2\left(b_3 + b'\right)t_c \tag{A-24}$$

which is rewritten as

$$\frac{\tilde{t}_c}{t_c} = \frac{b_3 + b'}{\tilde{b} + b'} \tag{A-25}$$

which, through the application of $b_3 = b_4$ and equations (A-14) and (A-22), leads to

$$\frac{\tilde{t}_c}{t_c} = \frac{3 + \sqrt{2}}{3\sqrt{1 + 24\frac{h_c^2}{b_4^2}} + \sqrt{2}} = \frac{3 + \sqrt{2}}{3\sqrt{1 + 256\frac{h_c^2}{d_4^2}} + \sqrt{2}} \quad ; \quad b_4 = \frac{3\sqrt{2}}{8}d_4 \tag{A-26}$$

Substituting equation (A-26) into equation (A-23) yields

$$\frac{\rho_4}{\rho_c} = \frac{A_w^{(4)}}{A_c^{(4)}} = \frac{2(3+\sqrt{2})t_c}{5b_4} = \frac{8\sqrt{2}(3+\sqrt{2})t_c}{15d_4} \quad ; \quad b_4 = \frac{3\sqrt{2}}{8}d_4 \tag{A-27}$$

which is similar to equation (A-13) (the flat cell wall case, $i = 3$).

NOTE

This report stemmed from the investigations of heat shielding and thermoelastic performance of superalloy thermal protection system (TPS) to be used for protecting the X-33 research vehicle from overheating during its mission. The report contains no classified information, and serves as a stimulant for university professors and their graduate students to extend Ko's basic research work.

William L. Ko
April 27, 2000

Material Properties

Table A-1. Material properties of Inconel 617 used for superalloy TPS panel.

T, °F	450	625	800	1800	2000
E, lb/in^2	28.25×10^6	27.50×10^6	26.50×10^6	18.20×10^6	16.0×10^6
G, lb/in^2	11.00×10^6	10.60×10^6	10.20×10^6	6.60×10^6	5.71×10^6
ν	0.284	0.297	0.300	0.390	0.400
α, in/in–°F	7.12×10^{-6}	7.50×10^{-6}	7.65×10^{-6}	9.10×10^{-6}	9.25×10^{-6}
ρ_c, lb/in^3	0.3015	0.3015	0.3015	0.3015	0.3015

REFERENCES

1. Ko, William L., Robert D. Quinn, and Leslie Gong, *Finite-Element Reentry Heat Transfer Analysis of Space Shuttle Orbiter*, NASA TP-2657, 1986.

2. Ransone, Philip O. and Donald R. Rummler, *Microstructural Characterization of the HRSI Thermal Protection System for Space Shuttle*, NASA TM-81821, 1980.

3. Pusch, R. H., *Thermal Insulation Blanket Material*, NASA CR-166367, 1982.

4. Blair, Winford, John E. Meaney, and Herman A. Rosenthal, *Design and Fabrication of Titanium Multi-Wall Thermal Protection System (TPS) Test Panels*, NASA CR-159241, 1980.

5. Blair, W., *Fabrication of Titanium Multiwall Thermal Protection System (TPS) Curved Panel*, NASA CR-165754, 1981.

6. Blair, W., J. E. Meaney, and H. A. Rosenthal, *Fabrication of Prepackaged Superalloy Honeycomb Thermal Protection System (TPS) Panels*, NASA CR-3755, 1985.

7. Shideler, J. L., G. L. Webb, and C. M. Pittman, "Verification Tests of Durable Thermal Protection System Concepts," *J. Spacecraft and Rockets*, vol. 22, no. 6, Nov–Dec., 1985, pp. 598–604.

8. Williams, S. D. and Donald M. Curry, *Thermal Protection Materials—Thermophysical Property Data*, NASA Reference Publication 1289, 1992.

9. Noor, Ahmed K., W. Scott Burton, and Charles W. Bert, "Computational Models for Sandwich Panels and Shells," *Applied Mechanics Reviews*, vol. 49, no. 3, Mar. 1996, available as ASME Reprint no. 186.

10. Whetstone, W. D., *SPAR Structural Analysis System Reference Manual, System Level 13A: Volume 1, Program Execution*, NASA CR-158970-1, 1978.

11. Brown, William F., Jr., Harold Mindlin, and C. Y. Ho, *Aerospace Structural Metals Handbook*, CINDAS/USAF CRDA Handbook Operation, Purdue University, 1997 Edition.

12. Ko, William L., *Thermostructural Behavior of a Hypersonic Aircraft Sandwich Panel Subjected to Heating on One Side*, NASA TM-4769, 1997.

13. Ko, William L., *Elastic Constants for Superplastically Formed/Diffusion-Bonded Corrugated Sandwich Core*, NASA TP-1562, 1980.

14. Timoshenko, Stephen P. and James M. Gere, *Theory of Elastic Stability*, Second Edition, McGraw-Hill Book Company, New York, 1961.

15. Ko, William L., *Mechanical and Thermal Buckling Analysis of Rectangular Sandwich Panels Under Different Edge Conditions*, NASA TM-4585, 1994.

REPORT DOCUMENTATION PAGE

Form Approved
OMB No. 0704-0188

1. AGENCY USE ONLY (Leave blank)	2. REPORT DATE	3. REPORT TYPE AND DATES COVERED
	May 2004	Technical Publication

4. TITLE AND SUBTITLE

Heat Shielding Characteristics and Thermostructural Performance of a Superalloy Honeycomb Sandwich Thermal Protection System (TPS)

5. FUNDING NUMBERS

WU 242-33-02-E8-23-00-TA1

6. AUTHOR(S)

William L. Ko

7. PERFORMING ORGANIZATION NAME(S) AND ADDRESS(ES)

NASA Dryden Flight Research Center
P.O. Box 273
Edwards, California 93523-0273

8. PERFORMING ORGANIZATION REPORT NUMBER

H-2492

9. SPONSORING/MONITORING AGENCY NAME(S) AND ADDRESS(ES)

National Aeronautics and Space Administration
Washington, DC 20546-0001

10. SPONSORING/MONITORING AGENCY REPORT NUMBER

NASA/TP-2004-212024

11. SUPPLEMENTARY NOTES

12a. DISTRIBUTION/AVAILABILITY STATEMENT

Unclassified—Unlimited
Subject Category 39

This report is available at http://www.dfrc.nasa.gov/DTRS/

12b. DISTRIBUTION CODE

13. ABSTRACT (Maximum 200 words)

Heat-transfer, thermal bending, and mechanical buckling analyses have been performed on a superalloy “honeycomb” thermal protection system (TPS) for future hypersonic flight vehicles. The studies focus on the effect of honeycomb cell geometry on the TPS heat-shielding performance, honeycomb cell wall buckling characteristics, and the effect of boundary conditions on the TPS thermal bending behavior. The results of the study show that the heat-shielding performance of a TPS panel is very sensitive to change in honeycomb core depth, but insensitive to change in honeycomb cell cross-sectional shape. The thermal deformations and thermal stresses in the TPS panel are found to be very sensitive to the edge support conditions. Slight corrugation of the honeycomb cell walls can greatly increase their buckling strength.

14. SUBJECT TERMS

Heat shielding performance, Heat transfer, Honeycomb sandwich panels, Thermal buckling, Thermal protection system

15. NUMBER OF PAGES

45

16. PRICE CODE

17. SECURITY CLASSIFICATION OF REPORT	18. SECURITY CLASSIFICATION OF THIS PAGE	19. SECURITY CLASSIFICATION OF ABSTRACT	20. LIMITATION OF ABSTRACT
Unclassified	Unclassified	Unclassified	Unlimited